

**Manuscript version: Author's Accepted Manuscript**

The version presented in WRAP is the author's accepted manuscript and may differ from the published version or Version of Record.

**Persistent WRAP URL:**

<http://wrap.warwick.ac.uk/102654>

**How to cite:**

Please refer to published version for the most recent bibliographic citation information. If a published version is known of, the repository item page linked to above, will contain details on accessing it.

**Copyright and reuse:**

The Warwick Research Archive Portal (WRAP) makes this work by researchers of the University of Warwick available open access under the following conditions.

© 2018 Elsevier. Licensed under the Creative Commons Attribution-NonCommercial-NoDerivatives 4.0 International <http://creativecommons.org/licenses/by-nc-nd/4.0/>.



**Publisher's statement:**

Please refer to the repository item page, publisher's statement section, for further information.

For more information, please contact the WRAP Team at: [wrap@warwick.ac.uk](mailto:wrap@warwick.ac.uk).

1 ***Drosophila* TNF modulates tissue tension in the embryo to facilitate macrophage**  
2 **invasive migration**

3 *Aparna Ratheesh,<sup>1</sup> Julia Biebl,<sup>1</sup> Jana Vesela,<sup>1</sup> Michael Smutny,<sup>1,2</sup> Ekaterina*  
4 *Papusheva,<sup>1</sup> S.F. Gabriel Krens,<sup>1</sup> Walter Kaufmann,<sup>1</sup> Attila Gyoergy,<sup>1</sup> Alessandra*  
5 *Maria Casano,<sup>1,3</sup> and Daria E. Siekhaus<sup>1,4,\*</sup> ORCID*

6 <sup>1</sup>*Institute of Science and Technology Austria, Am Campus 1, 3400 Klosterneuburg,*  
7 *Austria*

8 <sup>2</sup>*Centre for Mechanochemical Cell Biology and Division of Biomedical Sciences,*  
9 *Warwick Medical School, University of Warwick, Coventry CV47AL*

10 <sup>3</sup>*EMBL Heidelberg, Meyerhofstraße 1, 69117 Heidelberg, Germany*

11

12

13 Corresponding Author: Daria Siekhaus, [daria.siekhaus@ist.ac.at](mailto:daria.siekhaus@ist.ac.at)

14 Lead Contact: Daria Siekhaus, [daria.siekhaus@ist.ac.at](mailto:daria.siekhaus@ist.ac.at)

15

16

17

18

19

20

21

22

23

24

25

26 **Summary:**

27 Migrating cells penetrate tissue barriers during development, inflammatory responses  
28 and tumor metastasis. We study if migration *in vivo* in such three-dimensionally  
29 confined environments requires changes in the mechanical properties of the  
30 surrounding cells using embryonic *Drosophila melanogaster* hemocytes, also called  
31 macrophages, as a model. We find that macrophage invasion into the germband  
32 through transient separation of the apposing ectoderm and mesoderm requires cell  
33 deformations and reductions in apical tension in the ectoderm. Interestingly, the  
34 genetic pathway governing these mechanical shifts acts downstream of the only  
35 known TNF superfamily member in *Drosophila*, Eiger, and its receptor, Grindelwald.  
36 Eiger-Grindelwald signaling reduces levels of active Myosin in the germband  
37 ectodermal cortex through the localization of a Crumbs complex component, Patj  
38 (Pals-1-associated tight junction protein). We therefore elucidate a distinct molecular  
39 pathway that controls tissue tension and demonstrate the importance of such  
40 regulation for invasive migration *in vivo*.

41

42 **Keywords:**

43 hemocytes, plasmatocytes, macrophages, immune cell, Eiger, Grindelwald, TNF,  
44 *Drosophila*, Patj, Crumbs, Myosin, tension, invasion, migration

45

46

47

48

49

50

## 51 **Introduction**

52 A full understanding of migration in the complex three-dimensional environment that  
53 exists *in vivo* requires investigating how cells move through the mechanical  
54 constraints posed by their surroundings. A number of studies have recently shown that  
55 increased stiffness of the matrix promotes invasion by cancer and immune cells  
56 (Friedl et al., 2012; Laklai et al., 2016; Levental et al., 2009; Miroshnikova et al.,  
57 2016) but little research has been conducted *in vivo* on the influence of the  
58 mechanical properties of neighboring tissues. We address such questions using the  
59 migration of *Drosophila* plasmatocytes in the embryo. Plasmatocytes, also called  
60 hemocytes, are the primary phagocytic cells in the *Drosophila* embryo and share  
61 striking similarities with vertebrate macrophages in ontogeny, functionality and  
62 migratory behavior (Evans and Wood, 2011; Gold and Brückner, 2014; Lemaitre and  
63 Hoffmann, 2007; Nourshargh et al., 2010; Ratheesh et al., 2015; Reymond et al.,  
64 2013; Vestweber, 2015; Weavers et al., 2016). They are specified in the head  
65 mesoderm at embryonic Stages 4-6 and at Stage 9 they start migrating along pre-  
66 determined paths following cues from the PDGF- and VEGF-related factors (Pvf) 2  
67 and 3 (Brückner et al., 2004; Cho et al., 2002; Evans and Wood, 2011; Gold and  
68 Brückner, 2014; Siekhaus et al., 2010; Weavers et al., 2016) to populate the entire  
69 embryo (Figure 1A). One of these early migratory routes stretches from the head  
70 mesoderm across the yolk sac and into the extended germband (blue arrow, Figure  
71 1A) (Ratheesh et al., 2015; Siekhaus et al., 2010) that undergoes retraction to the  
72 posterior of the embryo by late Stage 12. Our previous work demonstrated that this  
73 germband route requires macrophage movement through a tissue barrier and displays  
74 molecular parallels to vertebrate immune cell transmigration in its requirement for  
75 modulation of Integrin affinity through small GTPases in macrophages (Siekhaus et

76 al., 2010). In this study we unravel the molecular and mechanical changes that occur  
77 in the germband to promote this macrophage tissue invasion.

78

## 79 **Results**

### 80 *Macrophages invade the germband between the closely apposed epithelial ectoderm* 81 *and mesoderm*

82 We first examined in detail the environment of macrophage migration into the  
83 germband as well as the nature of the constraints that they might encounter in the  
84 process. We performed two-photon imaging in Stage 11 embryos, labeling both the  
85 macrophages as well as the surrounding tissues and focusing on the region of the  
86 germband (Figure 1B). At this stage they migrated on top of the yolk sac. While a few  
87 macrophages migrated into the folds of the amnioserosa (yellow arrow, Figure 1C and  
88 S1), the majority moved further along the yolk sac and entered the germband (Figure  
89 S1A,B and Movie S1). Migration into the germband at late Stage 11 appeared to be a  
90 multi-step, time intensive process during which the initial macrophage first inserted a  
91 protrusion into and between the cells of the germband (Figure 1C, white arrow). This  
92 protrusion enlarged as the initial macrophage fully penetrated the germband (Figure  
93 1C arrowhead and Movie S1) followed closely by the remaining macrophages.  
94 Macrophages invariably entered the germband at specific locations (Figure 1C and  
95 Movie S1) which confocal imaging of fixed Stage 12 embryos revealed to be where  
96 ectoderm expressing DE-Cadherin abuts visceral mesoderm expressing DN-Cadherin  
97 (Figure 1D). Macrophages continue to migrate along this ectoderm-mesoderm  
98 interface during Stage 12 (Figure 1D). Prior to macrophage entry the ectodermal  
99 epithelium and the mesoderm lie closely apposed to one another (Figure 1D merge,  
100 Figure 1E arrows). During macrophage entry into the germband, the two tissues

101 separate concomitantly with macrophage entry and the macrophages migrate onwards  
102 while confined between them (Figure 1D,E, Figure S1A,B and Movie S1).

103 To examine this tissue interface in more detail we used transmission electron  
104 microscopy (TEM), identifying the ectoderm and the mesoderm using their  
105 morphology, with the outer ectoderm cells having a typical columnar appearance and  
106 the inner mesoderm cells appearing more rounded. TEM images confirmed that the  
107 two tissues lie in close proximity prior to macrophage entry (Figure S1C,D, Figure  
108 1F-H) matching our observation that macrophages are not utilizing pre-existing gaps  
109 in the germband to enter. Close examination of the germband ectoderm prior to entry  
110 revealed that ectodermal cells are organized in a polarized epithelium, with Adherens  
111 junctions (AJ) facing the outside of the germband (Figure S1D, E), and the basal side  
112 of the ectoderm forming an interface with the adjacent mesoderm. Previous studies  
113 have shown that Collagen is deposited at significant levels during later embryonic  
114 stages (Matsubayashi et al., 2017) however we found that the mesoderm starts  
115 secreting Laminin A (LanA) in Stage 11, resulting in visible deposition at the  
116 interface of the ectoderm and mesoderm (Figure 1I,J) by the time macrophages  
117 prepare to enter the germband. Previous studies have shown that Matrix  
118 Metalloproteases are not required for macrophage migration into the germband  
119 (Siekhaus et al., 2010), suggesting that while macrophages might utilize Laminin as a  
120 substrate during migration, ECM cleavage is not needed for macrophage entry. Our  
121 data show that embryonic macrophages intercalate between previously closely  
122 apposed tissues as they enter and continue moving within the germband (Figure 1K,  
123 Figure S1A,B and Movie S1) indicating that this system is ideally suited to  
124 understand the three-dimensional mechanical constraints extant during tissue invasion  
125 *in vivo*.

126 *Eiger in the amnioserosa is required for macrophage invasion into the extended*  
127 *germband*

128 To identify the molecular pathways that could modulate mechanical parameters  
129 during germband invasion we searched for genes expressed in and around the tissues  
130 which macrophages enter. Given that vertebrate TNF $\alpha$  facilitates leukocyte ingressions  
131 between vascular endothelial cells, we focused on Eiger (EDA-like cell death trigger),  
132 the sole *Drosophila* member of the Tumor Necrosis Factor (TNF) superfamily (Igaki,  
133 2002; Kanda et al., 2002) which is expressed in the amnioserosal tissue that lies  
134 adjacent to the germband (Figure 2A, arrow) as well as along the ventral nerve cord.  
135 We tested if Eiger was important for macrophage migration into and within the  
136 germband by assessing the numbers of macrophages inside the germband in embryos  
137 from the *eiger* excision mutants, *egr<sup>1</sup>* and *egr<sup>3</sup>*, which remove the promoter as well as  
138 the translational start site (Igaki, 2002). To be sure that any differences in macrophage  
139 numbers between genotypes were not due to differences in staging, we examined  
140 embryos with 35-40% retraction of the germband from the anterior, a discrete time  
141 period during Stage 12 (Figure S2A). Fixed embryos from *egr<sup>1</sup>* and *egr<sup>3</sup>* mutant flies  
142 displayed a 50% decrease in the number of macrophages in the germband compared  
143 to the control, visualized using a macrophage specific driver (Figure 2B-D and Figure  
144 S2A). The *egr<sup>1</sup>* phenotype was not enhanced over the deficiency Df(2R)BSC303 that  
145 completely removes the gene (Figure 2D) and *egr<sup>1</sup>* embryos displayed no expression  
146 of the gene (Figure 2A). This evidence suggests that *egr<sup>1</sup>* is a null allele and we  
147 therefore used this mutant in all of our further experiments. Changes in the timing of  
148 the initiation of the developmental movements of the germband or the speed with  
149 which these steps occur could have affected our assessment of macrophage numbers  
150 in the germband. Hence we imaged the germband live in control and *egr<sup>1</sup>* embryos

151 and found no significant difference either in when germband extension was initiated  
152 (192 $\pm$ 2 minutes after fertilization (AF) for control and 194 $\pm$ 2 minutes AF for *egr<sup>l</sup>*) or  
153 the time taken for its completion (34 $\pm$ 1 minutes for control and 34 $\pm$ 2 minutes for *egr<sup>l</sup>*  
154 embryos, n=17 embryos for both genotypes). We also found no significant difference  
155 either in when germband retraction began (Figure S2B), the time taken for the initial  
156 phase of retraction to 35-41% of egg length (Figure S2C) or for its full completion  
157 (122 $\pm$ 4 minutes for control and 121 $\pm$ 3 minutes for *egr<sup>l</sup>*, n=16 embryos for control and  
158 17 embryos for *egr<sup>l</sup>*). We therefore concluded that Eiger directly regulates the number  
159 of macrophages that migrate into the germband. The amnioserosa (AS) appeared to be  
160 the predominant source of the Eiger that affects macrophage tissue invasion;  
161 expressing *eiger* in the AS significantly rescued the *egr<sup>l</sup>* phenotype and driving an  
162 RNAi construct against *eiger* in the AS substantially recapitulated the *egr<sup>l</sup>* phenotype  
163 (Figure 2E,F and Figure S2D,E). *egr<sup>l</sup>* embryos displayed no changes in the number of  
164 macrophages migrating along the ventral nerve cord (vnc) (Figure S2F,G,H) or in the  
165 number of macrophages that end up in the anterior tip of the head (Figure S2I,J).  
166 There was also no change in the total number of macrophages (Figure S2K), arguing  
167 that Eiger acts specifically to affect macrophage migration into or within the  
168 germband but not their movement along other routes, survival or division.  
169 To confirm this conclusion we directly assessed the migratory properties of  
170 macrophages in the *egr<sup>l</sup>* null mutant. We performed two-photon imaging in live  
171 *Drosophila* embryos with sufficient spatial and temporal resolution to allow us to  
172 segment and track the macrophage nuclei in 4D (Movie S2 & 3). We observed no  
173 significant change in speed during macrophage migration from the head up to the  
174 germband when compared to the control and a small (7%) decrease in the persistence  
175 (Figure 2G-I and Figure S2L,M). The conclusion that Eiger does not impede



176 migratory steps prior to germband entry was further supported by the observation in  
177 both fixed analysis and live imaging of *egr<sup>1</sup>* mutant embryos that macrophages  
178 accumulated at the edge of the germband (Figure 2B,J (arrows), and Movie S2). We  
179 therefore imaged macrophage entry into the germband in embryos in which  
180 macrophages were visualized with cytoplasmic mCherry and the ectoderm was  
181 labeled with *knock-in DE-Cadherin::GFP* (Huang et al., 2009). Macrophages paused  
182 at the germband edge with the first macrophage taking ~30 min to move in after  
183 initial contact (Figure 2K and Movie S4), confirming our initial assessment that  
184 macrophage entry into the germband is a time-intensive process. In *egr<sup>1</sup>* mutants,  
185 germband entry took even longer, requiring 60% more time (~50 min, Figure 2K).  
186 We went on to assess whether Eiger also affects macrophage migration within the  
187 germband. Interestingly we found that the speed of migration of the first macrophage  
188 in the area of germband which lies in contact or very close to the AS (Figure 2L), is  
189 significantly slower in *egr<sup>1</sup>* mutant embryos compared to the control, yet the speed  
190 thereafter did not show a significant difference (Figure 2M,N Figure S2N,O). This  
191 suggests that Eiger expression in the AS controls macrophage migration within the  
192 region of the germband that lies adjacent to the AS. Thus we show that, like  
193 vertebrate TNF, the *Drosophila* TNF, Eiger can regulate immune cell tissue invasion,  
194 facilitating invasive entry and initial invasive migration.

195 ***The TNF receptor Grindelwald in the ectoderm regulates macrophage tissue***  
196 ***invasion but not general migration***

197 We asked how Eiger, which is expressed in the AS, could regulate macrophage  
198 migration into and within the neighboring germband. Confocal imaging of antibody  
199 staining against Eiger in Stage 10 embryos, in which macrophages do not contact the  
200 amnioserosa or germband, revealed Eiger localized in puncta at the membrane of the

201 AS cells (Figure 3A, arrowhead in Figure 3A' and Figure S3A, arrowhead in Figure  
202 S3A'). However, at Stage 11, in which embryos displayed germband retraction of 29-  
203 31% and macrophages had reached the AS and the germband, Eiger staining was  
204 much lower in the AS (Figure 3B,C, Figure S3B, arrowhead in Figure S3B'), and  
205 became evident on the germband ectoderm (arrow in Figure 3B'), displaying a three  
206 fold increase when quantitated (Figure 3D), as well as becoming detectable on other  
207 surrounding tissues. This suggested that Eiger is released from the AS cells in a  
208 developmentally timed process that correlates with macrophage germband invasion.  
209 Our data is consistent with previous studies which have shown that Eiger, like other  
210 TNFs, can undergo proteolytic cleavage to permit release and diffusion of the  
211 extracellular domain from the cell surface (Agrawal et al., 2016; Jo et al., 2017;  
212 Kauppila et al., 2003). We next looked for potential Eiger receptors expressed in the  
213 germband that could mediate its role in macrophage tissue invasion. Interestingly, the  
214 transcript encoding Grindelwald, a transmembrane protein with homology to  
215 members of the TNFR superfamily, is expressed at high levels in the germband  
216 ectoderm in Stage 11 embryos with weaker expression throughout the caudal  
217 ectoderm (Figure 3E). Grindelwald has recently been shown to act as an Eiger  
218 receptor, binding Eiger through its TNF homology domain and mediating its pro-  
219 apoptotic and signaling functions (Andersen et al., 2015). Ectodermal knockdown of  
220 *grindelwald* using tissue specific RNAi resulted in a decrease in the number of  
221 macrophages in the germband (Figure 3F), suggesting that Grindelwald functions in  
222 the ectoderm to support macrophage tissue invasion. We then tested the effect of a  
223 *grindelwald* null mutant (Andersen et al., 2015), *grnd*<sup>Minos</sup>, on macrophage migration.  
224 Similarly to *egr*<sup>1</sup>, *grnd*<sup>Minos</sup> embryos showed a significant decrease in the number of  
225 macrophages in the germband compared to the control (Figure 3G). This change was

226 not due to a decrease in the total number of macrophages, since that was unaffected in  
227 *grnd<sup>Minos</sup>* (Figure S3C). Live imaging and tracking of macrophage nuclei  
228 demonstrated that the speed and persistence of macrophage migration up to the  
229 germband was unaffected in the *grnd<sup>Minos</sup>* mutant compared to the control (Figure 3H,  
230 Figure S3D-G and Movie S3). There was also no significant change in macrophage  
231 numbers along the vnc suggesting that, like Eiger, Grindelwald does not affect the  
232 general migratory properties of macrophages (Figure S3H,I). Taken together this data  
233 suggests that Eiger is released from AS cells and acts on the neighboring germband  
234 ectodermal epithelium through its interaction with Grindelwald to facilitate  
235 macrophage tissue invasion.

236 ***Eiger does not regulate E or N-Cadherin or cell-ECM signaling at the ectoderm-***  
237 ***mesoderm interface***

238 We analyzed whether Eiger signaling might facilitate macrophage tissue invasion into  
239 and within the first part of the germband by lowering the levels of adhesion molecules  
240 present at the ectoderm-mesoderm interface in this region. To examine this, we  
241 assessed wild type and *egr<sup>l</sup>* mutant embryos both at Stage 10, before the release of  
242 Eiger from the amnioserosa, and at Stage 11, when Eiger appears on the ectoderm and  
243 macrophages contact the germband. We found no significant difference between wild  
244 type and *egr<sup>l</sup>* mutant embryos in DE-Cadherin or DN-Cadherin levels at either stage,  
245 suggesting that increased coupling between the two adhesion molecules and thus the  
246 two tissues could not account for the *egr<sup>l</sup>* phenotype (Figure S4A-C and Figure 4B-  
247 D). We then looked for potential changes in the interactions of ectodermal cells with  
248 the ECM that lies on its basal side, at the interface with the mesoderm, in *egr<sup>l</sup>*  
249 mutants compared to wild type. We observed no change at either stage between  
250 control and *egr<sup>l</sup>* mutants in the levels of accumulation at the ectoderm-mesoderm

251 interface of Laminin A (Lan A) or its potential receptors Dystroglycan (Deng et al.,  
252 2003) and Myospheroid which is the common Integrin  $\beta$  subunit present in flies, or  
253 Talin which is essential for linking ligand-bound Integrins to the cytoskeleton and  
254 focal adhesion assembly (Brown et al., 2002; Ellis et al., 2014; Klapholz et al., 2015)  
255 (Figure 4E-K, Figure S4D-K). Our data shows that Eiger does not regulate levels of  
256 Lan A or its receptors at the ectoderm-mesoderm interface, but do not preclude  
257 changes in signaling that we did not assess. We also did not see any significant  
258 change between Stages 10 and 11 in wild type embryos at the ectoderm-mesoderm  
259 interface in the levels of E- or N-Cadherin, Dystroglycan, Myospheroid or Talin  
260 (Figure S4L). The one protein for which we did see a difference was LanA, which  
261 increased in Stage 11 compared to Stage 10 both at the ectoderm-mesoderm interface  
262 (Supplementary Figure 4L) as well as within the mesoderm (Figure S4M). This LanA  
263 increase was not Eiger dependent since we saw a similar increase in the *egr<sup>1</sup>* mutant  
264 embryos (Figure S4L,M). These findings argue that Eiger does not regulate Cadherin  
265 or Integrin mediated adhesion at the ectoderm-mesoderm interface to facilitate  
266 macrophage tissue invasion.

267 ***Eiger maintains apical Pals1-associated tight junction (PATJ) to regulate myosin***  
268 ***activity in the ectoderm without affecting polarity during macrophage tissue***  
269 ***invasion***

270 The known ability of Eiger, when overexpressed in the imaginal discs, to activate  
271 apoptosis through JNK (Jun amino terminal kinase) signaling (Andersen et al., 2015;  
272 Igaki, 2002; Moreno et al., 2002) led us to examine these potential responses to Eiger  
273 signaling in the germband. However the level of Caspase mediated apoptosis in the  
274 germband was unaffected in both *egr<sup>1</sup>* and *grnd<sup>Minos</sup>* embryos compared to the control  
275 (Figure 5A, Figure S5A). We then assessed JNK signaling using the *Puc<sup>E69</sup>-GAL4*

276 crossed to *UAS-GFP* as a reporter line (Adachi-Yamada, 2002). In control embryos, a  
277 few cells in the AS showed expression of the JNK reporter, yet none did so in the  
278 germband ectodermal epithelium (Figure S5B), and the expression level did not  
279 change significantly in *egr<sup>1</sup>* embryos compared to controls (Figure S5C). We therefore  
280 concluded that Eiger does not regulate macrophage tissue invasion through canonical  
281 JNK signaling and activation of apoptosis.

282 We then turned our attention to the apical side of the germband ectoderm which is in  
283 close contact with the amnioserosa where Eiger is expressed. Grindelwald has been  
284 shown to interact with the Crumbs apical polarity complex (Andersen et al., 2015).  
285 The complex consists of the transmembrane protein Crumbs, its adaptor protein  
286 Stardust, and the Stardust associated proteins Patj (Pals1-associated tight junction)  
287 (Bachmann et al., 2008; Bulgakova et al., 2008; Sen et al., 2015) and Veli (Lin-7)  
288 which Grindelwald can directly bind (Fig 6I, left panel) (Andersen et al., 2015). To  
289 test the importance of Veli in our system, we knocked it down in the ectoderm with  
290 RNAi and observed a defect in the number of macrophages within the germband  
291 (Figure 5B); this result supports the hypothesis that the association of Grindelwald  
292 with the Crumbs complex through Veli is important for the regulation of macrophage  
293 tissue invasion. Based on this, we tested if the Eiger-Grindelwald complex might  
294 regulate the action of members of the Crumbs complex in the germband ectoderm.  
295 Crumbs was apically localized in a pattern similar to the control in *egr<sup>1</sup>* and *grnd<sup>Minos</sup>*  
296 mutant Stage 12 embryos and quantification of apical Crumbs levels showed no  
297 significant difference between the control embryos and the *egr<sup>1</sup>* or *grnd<sup>Minos</sup>* mutant  
298 embryos suggesting that ectodermal apical polarity was unaffected (Figure 5D,E and  
299 Figure S5D). However, we detected a strong reduction in the apical localization of  
300 Patj in both *egr<sup>1</sup>* and *grnd<sup>Minos</sup>* embryos (Figure 5F,G and Figure S5D). Importantly,

301 overexpressing *patj* using an ectodermal driver rescued the macrophage germband  
302 migration defect in *egr<sup>1</sup>* embryos (Figure 5J,K), supporting the idea that the defect in  
303 macrophage invasion in *egr<sup>1</sup>* embryos is significantly caused by the loss of Patj.  
304 Next we examined how the loss of apical Patj could affect the germband ectodermal  
305 epithelium, and ultimately macrophage migration. Patj has been shown to bind the  
306 Myosin binding subunit (MBS) of Myosin phosphatase (Sen et al., 2012) which  
307 downregulates Myosin activity by decreasing its phosphorylation (Kimura et al.,  
308 1996; Lee and Treisman, 2004). Although no antibody for Myosin phosphatase exists,  
309 we were able to analyze the localization and levels of active Myosin in the ectoderm  
310 using an antibody that detects the mono-phosphorylated form of Myosin regulatory  
311 light chain (MRLC, *sqh* in *Drosophila*) (Zhang and Ward, 2011). We found a strong  
312 increase in the level of apical junctional phospho-MRLC in both *egr<sup>1</sup>* and *grnd<sup>Minos</sup>*  
313 mutant embryos compared to controls in the region of the germband ectoderm along  
314 which the first macrophage to enter migrates more slowly in the *egr<sup>1</sup>* mutant (Figure  
315 5H,I and Figure S5D). There was also a significant decrease in the levels of apical  
316 phospho-Myosin seen in wild type embryos from Stage 10 to early Stage 11 within  
317 this region suggesting that the shift in Eiger localization from the amnioserosa to the  
318 germband observed between these two stages (Figure S5E,F) reduces apical phospho-  
319 Myosin levels. Finally, to test if the increased active Myosin seen in the *egr<sup>1</sup>* mutants  
320 contributes to the defect in macrophage migration, we lowered Myosin levels in the  
321 ectoderm in *egr<sup>1</sup>* mutant embryos using RNAi against *MRLC (sqh)* and were able to  
322 significantly rescue the *egr<sup>1</sup>* phenotype (Figure 5J,K). This suggests that Eiger and  
323 Grindelwald facilitate macrophage invasion into and within the germband by  
324 maintaining apical Patj in the ectodermal epithelium, thus promoting a reduction in  
325 the levels of apical activated Myosin without affecting polarity.

326 *Eiger regulates ectodermal apical tension and tissue deformation to facilitate*  
327 *macrophage invasion*

328 As Myosin activity is known to affect cellular tension (Fernandez-Gonzalez et al.,  
329 2009) we tested if increased apical phospho-MRLC correlated with increased cortical  
330 tension. We conducted apical laser ablation in the germband ectoderm (Figure S6A)  
331 in control, *egr<sup>1</sup>*, and *grnd<sup>Minos</sup>* mutant embryos carrying *knock-in DE-Cadherin::GFP*  
332 to visualize the apical cortex of ectodermal cells. The laser intensity was standardized  
333 to ensure ablation of the apical Cadherin without the induction of significant damage  
334 to the embryos, which remained viable after the experiment. We measured the initial  
335 recoil velocity after the cut, which is indicative of the inherent apical tension at that  
336 location. Embryos from both mutants displayed higher recoil velocity indicating  
337 higher apical tension in the germband ectoderm compared to control embryos (Figure  
338 6A-E, and Movie S5). This increased tension was Myosin dependent, as it was  
339 eliminated in the presence of the Rho kinase inhibitor Y27632 (Figure 6F).

340 We then went on to examine the net interfacial tension along the apical edge of the  
341 ectoderm cells using a recently described force inference method, named CellFIT-3D  
342 (Brodland et al., 2014; Krens et al., 2017), which assesses interfacial tension  
343 distributions based on the angles present between contacting cell surfaces at triple cell  
344 junctions (Figure S6B). We performed CellFIT-3D analysis on high-resolution 3D  
345 confocal images of DE-Cadherin labeled fixed control and *egr<sup>1</sup>* mutant embryo stacks  
346 that were oversampled in the Z-axis, analyzing the apical, basal and lateral domains of  
347 the germband ectoderm. This force inference analysis indicated that while in control  
348 embryos both apical and basal tensions were approximately 1.8 times the lateral  
349 tension, in *egr<sup>1</sup>* mutant embryos the apical tension was higher than both the lateral and  
350 the basal tensions (Figure S6D and Movie S6). This comparison of the distribution of

351 relative interfacial tensions is consistent with our laser ablation analysis, which  
352 indicates that Eiger decreases apical tension in the germband ectoderm.

353 To directly assess the role of tension in regulating macrophage migration into the  
354 germband, we overexpressed in the ectoderm constitutively active Rho1 (Rho1.V14),  
355 a positive regulator of Rok, the kinase that phosphorylates Myosin (Kaibuchi et al.,  
356 1999; Niederman and Pollard, 1975). The number of macrophages present in the  
357 germband was significantly decreased in these embryos (Figure 6G and Figure S6E),  
358 supporting the conclusion that high levels of ectodermal tension can impede  
359 macrophage invasion into and within the germband. We therefore conclude that Egr  
360 and Grnd-mediated regulation of activated Myosin levels and thus apical tension of  
361 the ectodermal epithelium is critical for normal macrophage tissue invasion.

362 Finally we asked how changes in ectodermal apical tension could mechanistically  
363 facilitate the entry and initial migration of macrophages, which move between the  
364 basal side of the ectodermal epithelium and the adjacent mesoderm. As increased  
365 tensions have been predicted theoretically and shown experimentally to increase  
366 effective tissue stiffness (Koenderink et al., 2009; Kollmannsberger et al., 2011;  
367 Lange and Fabry, 2013; Wang et al., 2002), we reasoned that macrophage tissue  
368 invasion might require tension-dependent deformation of the columnar ectodermal  
369 cells. To test this hypothesis, we analyzed whether deformation of the ectodermal  
370 cells accompany macrophage entry and initial migration within the germband. We  
371 quantified in live embryos the shape changes as a ratio of length/width (LWR) of all  
372 the ectodermal cells in a given plane within 10 $\mu$ m from the macrophage edge. In  
373 control embryos, ectodermal cells displayed a significant decrease in LWR during this  
374 time, consistent with the hypothesis that ectodermal cells undergo compression as the  
375 macrophage fully insinuates itself into the germband (Figure 6H, Figure S6F and



376 Movie S7). Crucially, this deformation was significantly less pronounced in the *egr<sup>1</sup>*  
377 mutant embryos (Figure 6H, Figure S6F and Movie S7) suggesting that the observed  
378 increase in apical tension of these ectodermal cells causes them to resist the  
379 deformation accompanying macrophage entry into and initial migration within the  
380 germband to a higher degree than in the control, thereby delaying the macrophages.  
381 Based on our results, we propose the following model for Eiger-Grindelwald  
382 signaling during macrophage germband entry and migration within the germband.  
383 Amnioserosal Eiger binding to ectodermal Grindelwald leads to an enrichment of the  
384 Myosin-Phosphatase-MBS-Patj complex at the apical cortex where it remains bound  
385 to the Crumbs polarity complex through its interaction with Veli and Stardust (Figure  
386 6I). This results in a reduction in apical phosphorylated Myosin and apical tension  
387 that allows ectodermal deformation and thus macrophage migration into and within  
388 the region of the germband that abuts the amnioserosa.

### 389 **Discussion**

390 Our studies indicate an ancient conserved role for the TNF family in aiding immune  
391 cells to cross a tissue barrier and suggest that this functionality and the mechanisms  
392 underlying it evolved even before the vasculature did. The *Drosophila melanogaster*  
393 TNF, Eiger, has been previously linked mostly to stress responses, aiding in adaptive  
394 reactions to infection (Schneider et al., 2007), tumors (Ohsawa et al., 2011; Parisi et  
395 al., 2014), starvation (Agrawal et al., 2016), and UV irradiation (Babcock et al.,  
396 2009). Eiger can also be coopted to promote tumor invasiveness in some  
397 circumstances (Cordero et al., 2010) while the Eiger receptor, Grindelwald, has been  
398 shown to cause neoplastic growth as a result of polarity defects (Andersen et al.,  
399 2015). These tumors are the result of the Crumbs complex signaling to Grindelwald to  
400 induce JNK activation independently of Eiger (Andersen et al., 2015). Our work

401 provides evidence that during normal development the communication flows in the  
402 reverse direction, with Eiger and Grindelwald required for alterations in the apical  
403 localization of components normally associated with the Crumbs complex (Sen et al.,  
404 2015). We also show that this relocalization of Patj correlates with reduced apical  
405 Myosin activity, which underlie the macrophage migration defects in the *eiger* mutant  
406 since raising Patj or lowering Myosin levels rescues the phenotype. We thus identify a  
407 previously unappreciated molecular pathway by which a TNF can act, and  
408 demonstrate its importance during *Drosophila* macrophage tissue invasion. Vertebrate  
409 TNF  $\alpha$  is known to facilitate leukocyte transmigration through the vasculature during  
410 inflammation (Sata, 1998). Previous studies treating human endothelial cells *in vitro*  
411 with 100 fold higher levels of TNF than normally found in the blood stream have  
412 detected increases in Myosin phosphorylation (Damas et al., 1989; McKenzie, 2007).  
413 In contrast we observe *in vivo* that endogenous amounts of Eiger decrease cortical  
414 phosphorylated Myosin. Investigating if the mechanisms we describe here for a TNF  
415 family member also function during vascular extravasation *in vivo* is an important  
416 area of future research.

417 Little is known about the modulation of mechanical constraints that occurs when cells  
418 penetrate between other cells during development (Montell, 2003; Seifert and  
419 Lehmann, 2012), metastasis (Friedl et al., 2012; Reymond et al., 2013) and  
420 inflammation (Nourshargh et al., 2010; Vestweber, 2015). Previous studies examining  
421 the effects of stiffness of a three-dimensional environment *in vivo* on cell migration  
422 have shown that increased ECM stiffness promotes invasion through stimulation of  
423 mechanotransduction in the invading cells (Calvo et al., 2013; Egeblad et al., 2010;  
424 Laklai et al., 2016; Levental et al., 2009). In these systems increased stiffness has  
425 been shown to affect MMP secretion and/or realignment of the matrix fibers by the

426 invading cells thus aiding invasive migration (Gaggioli et al., 2007). Our data stands  
427 in apparent contrast to these findings, as we discover that increased apical ectodermal  
428 tension in the *egr<sup>1</sup>* mutant leads to decreased macrophage ingression and migration  
429 within the germband. We have not measured ectodermal stiffness directly in the  
430 embryo, but have seen that in the absence of Eiger, ectodermal cells undergo less  
431 deformation as the macrophages enter, suggesting that the higher apical tension leads  
432 to an overall increase in the effective stiffness of the ectoderm potentially due to  
433 volume conservation. Tension has been shown to lead to strain stiffening (Koenderink  
434 et al., 2009; Kollmannsberger et al., 2011; Lange and Fabry, 2013; Wang et al., 2002)  
435 and we hypothesize that the increased tension on the apical side results in a stiffer  
436 cortex which acts as a “cap” resisting curving out of the ectoderm both during initial  
437 macrophage penetration and subsequent migration. This hypothesis is further  
438 supported by the observation that a decrease in macrophage migration speed is seen  
439 only as they migrate into and along the region of the germband where we detected an  
440 increase in the apical levels of phosphorylated Myosin in the *eiger* mutants. Our work  
441 suggests that previously identified mechanisms which enable invading cells to  
442 overcome the hindrance of a stiff ECM, such as matrix metalloprotease secretion or  
443 realignment of the matrix fibers (Gaggioli et al., 2007) are not sufficient when cells  
444 invade between other closely apposed cells.

445 We identify here a controlled developmental switch, which modulates these  
446 mechanical properties during *Drosophila* embryogenesis to facilitate macrophage  
447 tissue invasion of a complex tissue structure. While the Pvf guidance factors (Cho et  
448 al., 2002) and the border between the ectoderm and mesoderm appear to determine  
449 the location of the route taken by macrophages into and within the germband, our  
450 work suggests that Eiger helps set the timing and speed of this movement by releasing

451 the brake on macrophage entry and initial migration produced by higher cortical  
452 tension. Previous *in vitro* work has indicated that substrates that are too soft impede  
453 migration, by decreasing the ability of cells to exert the traction forces needed to  
454 move (Pelham and Wang, 1997; Saez et al., 2005). In our system it is possible that the  
455 macrophages migrate not on the ectoderm, but rather use the underlying ECM and  
456 mesoderm as a substrate to move forward. Hence the final migratory properties of the  
457 macrophages within the germband would depend not only on ectodermal stiffness, but  
458 on the mechanical properties of the ECM and mesoderm as well. Immune cell  
459 infiltration of solid tumors involves immune cell invasion into the tumor mass that  
460 consists of a multitude of components of varying mechanical properties including the  
461 ECM, stromal cells, angiogenic vessels and the tumor cells themselves. Our work  
462 demonstrates the importance of understanding the distinctions in the mechanical  
463 constraints exerted by each of these components in the *in vivo* environment cells  
464 traverse and the molecular mechanisms needed to alter each of them. Such a complete  
465 understanding of invasive migration has the potential to identify new strategies for  
466 treatment of autoimmunity and cancer in humans.

467

#### 468 **Author contribution**

469 AR and DS conceived of the project and AR, AMC and DS designed the experiments.  
470 AR, JB, JV and AMC performed experiments with support from AG who generated  
471 reagents and provided technical support. MS aided the laser ablation and migration  
472 analysis. EP wrote the Matlab script to permit segmentation and deformation analysis  
473 and aided with optimizing imaging protocols. GK performed CellFIT-3D analysis.  
474 WK optimized EM protocols. AR, MS, EP, AMC, and DS analyzed the data. AR and  
475 DS wrote the manuscript.

476

477 **Acknowledgements**

478 We thank K. Brueckner (UCSF, USA), M Galko (MD Anderson, USA), A Classen  
479 (LSM, Germany), M Miura (University of Tokyo, Japan), E Knust (MPI-CBG,  
480 Germany), P Leopold (IBV, France), R Ward (University of Kansas, USA), Y. Hong  
481 (U. Pittsburgh, USA), M. Krahn (U. Regensburg, Germany) for reagents, M. Sixt,  
482 C.P. Heisenberg and our laboratory members for scientific discussions and the former  
483 and M. Akhmanova, C. Guet, T. Hurd, E. Hannezo, P. Rangan, C. Schwayer, and A.  
484 Yap for comments on the manuscript. We utilized antibodies from the Developmental  
485 Studies Hybridoma Bank (The University of Iowa, USA) created by the NICHD of  
486 the NIH. Stocks obtained from the Bloomington *Drosophila* Stock Center (NIH  
487 P40OD018537) and the Vienna *Drosophila* Resource Center were used in this study.  
488 This work depended on information provided by FlyBase. We thank the Scientific  
489 Service Units at IST Austria for technical support. DS was supported by Marie Curie  
490 CIG 34077/IRTIM and AR by Marie Curie IIF GA-2012-32950 BB: DICJI. AR and  
491 AG were also supported by the Austrian Science Foundation (FWF)  
492 P\_DASI\_FWF01\_P29638. We are deeply grateful to Ruth Lehmann of NYU School  
493 of Medicine Skirball Center in whose lab the work underlying this research was  
494 begun.

495

496 **Declaration of Interests**

497 The authors declare no competing interests.

498

499 **References**

500

501 Adachi-Yamada, T. (2002). Puckered-GAL4 driving in JNK-active cells. *Genesis* 34,  
502 19–22.

- 503 Agrawal, N., Delanoue, R., Mauri, A., Basco, D., Pasco, M., Thorens, B., and  
504 Léopold, P. (2016). The *Drosophila* TNF Eiger Is an Adipokine that Acts on Insulin-  
505 Producing Cells to Mediate Nutrient Response. *Cell Metab.* *23*, 675–684.
- 506 Andersen, D.S., Colombani, J., Palmerini, V., Chakrabandhu, K., Boone, E.,  
507 Röthlisberger, M., Toggweiler, J., Basler, K., Mapelli, M., Hueber, A.-O., et al.  
508 (2015). The *Drosophila* TNF receptor Grindelwald couples loss of cell polarity and  
509 neoplastic growth. *Nature* *522*, 482–486.
- 510 Babcock, D.T., Landry, C., and Galko, M.J. (2009). Cytokine signaling mediates UV-  
511 induced nociceptive sensitization in *Drosophila* larvae. *Curr. Biol.* *19*, 799–806.
- 512 Bachmann, A., Grawe, F., Johnson, K., and Knust, E. (2008). *Drosophila* Lin-7 is a  
513 component of the Crumbs complex in epithelia and photoreceptor cells and prevents  
514 light-induced retinal degeneration. *Eur. J. Cell Biol.* *87*, 123–136.
- 515 Brodland, G.W., Veldhuis, J.H., Kim, S., Perrone, M., Mashburn, D., and Hutson,  
516 M.S. (2014). CellFIT: a cellular force-inference toolkit using curvilinear cell  
517 boundaries. *PLoS ONE* *9*, e99116.
- 518 Brower, D.L., Wilcox, M., Piovant, M., Smith, R.J., and Reger, L.A. (1984). Related  
519 cell-surface antigens expressed with positional specificity in *Drosophila* imaginal  
520 discs. *Proc. Natl. Acad. Sci. U.S.A.* *81*, 7485–7489.
- 521 Brown, N.H., Gregory, S.L., Rickoll, W.L., Fessler, L.I., Prout, M., White, R.A.H.,  
522 and Fristrom, J.W. (2002). Talin is essential for integrin function in *Drosophila*. *Dev.*  
523 *Cell* *3*, 569–579.
- 524 Brückner, K., Kockel, L., Duchek, P., Luque, C.M., Rørth, P., and Perrimon, N.  
525 (2004). The PDGF/VEGF receptor controls blood cell survival in *Drosophila*. *Dev.*  
526 *Cell* *7*, 73–84.
- 527 Bulgakova, N.A., Kempkens, O., and Knust, E. (2008). Multiple domains of Stardust  
528 differentially mediate localisation of the Crumbs-Stardust complex during  
529 photoreceptor development in *Drosophila*. *Journal of Cell Science* *121*, 2018–2026.
- 530 Calvo, F., Ege, N., Grande-Garcia, A., Hooper, S., Jenkins, R.P., Chaudhry, S.I.,  
531 Harrington, K., Williamson, P., Moeendarbary, E., Charras, G., et al. (2013).  
532 Mechanotransduction and YAP-dependent matrix remodelling is required for the  
533 generation and maintenance of cancer-associated fibroblasts. *Nat. Cell Biol.* *15*, 637–  
534 646.
- 535 Cho, N.K., Keyes, L., Johnson, E., Heller, J., Ryner, L., Karim, F., and Krasnow,  
536 M.A. (2002). Developmental control of blood cell migration by the *Drosophila* VEGF  
537 pathway. *Cell* *108*, 865–876.
- 538 Cordero, J.B., Macagno, J.P., Stefanatos, R.K., Strathdee, K.E., Cagan, R.L., and  
539 Vidal, M. (2010). Oncogenic Ras diverts a host TNF tumor suppressor activity into  
540 tumor promoter. *Dev. Cell* *18*, 999–1011.
- 541 Damas, P., Reuter, A., Gysen, P., Demonty, J., Lamy, M., and Franchimont, P.  
542 (1989). Tumor necrosis factor and interleukin-1 serum levels during severe sepsis in

- 543 humans. *Crit. Care Med.* *17*, 975–978.
- 544 Deng, W.-M., Schneider, M., Frock, R., Castillejo-Lopez, C., Gaman, E.A.,  
545 Baumgartner, S., and Ruohola-Baker, H. (2003). Dystroglycan is required for  
546 polarizing the epithelial cells and the oocyte in *Drosophila*. *Development* *130*, 173–  
547 184.
- 548 Egeblad, M., Nakasone, E.S., and Werb, Z. (2010). Tumors as organs: complex  
549 tissues that interface with the entire organism. *Dev. Cell* *18*, 884–901.
- 550 Ellis, S.J., Lostchuck, E., Goult, B.T., Bouaouina, M., Fairchild, M.J., López-  
551 Ceballos, P., Calderwood, D.A., and Tanentzapf, G. (2014). The talin head domain  
552 reinforces integrin-mediated adhesion by promoting adhesion complex stability and  
553 clustering. *PLoS Genet.* *10*, e1004756.
- 554 Evans, I.R., and Wood, W. (2011). *Drosophila* embryonic hemocytes. *Curr. Biol.* *21*,  
555 R173–R174.
- 556 Fernandez-Gonzalez, R., Simoes, S. de M., Röper, J.-C., Eaton, S., and Zallen, J.A.  
557 (2009). Myosin II dynamics are regulated by tension in intercalating cells. *Dev. Cell*  
558 *17*, 736–743.
- 559 Friedl, P., Locker, J., Sahai, E., and Segall, J.E. (2012). Classifying collective cancer  
560 cell invasion. *Nat. Cell Biol.* *14*, 777–783.
- 561 Gaggioli, C., Hooper, S., Hidalgo-Carcedo, C., Grosse, R., Marshall, J.F., Harrington,  
562 K., and Sahai, E. (2007). Fibroblast-led collective invasion of carcinoma cells with  
563 differing roles for RhoGTPases in leading and following cells. *Nat. Cell Biol.* *9*,  
564 1392–1400.
- 565 Gold, K.S., and Brückner, K. (2014). *Drosophila* as a model for the two myeloid  
566 blood cell systems in vertebrates. *Exp. Hematol.* *42*, 717–727.
- 567 Gyoergy, A., Roblek, M., Ratheesh, A., Valoskova, K., Belyaeva, V., Wachner, S.,  
568 Matsubayashi, Y., Sánchez-Sánchez, B.J., Stramer, B., and Siekhaus, D.E. (2018).  
569 Tools Allowing Independent Visualization and Genetic Manipulation of *Drosophila*  
570 *melanogaster* Macrophages and Surrounding Tissues. *G3 (Bethesda)* *8*, 845–857.
- 571 Huang, J., Zhou, W., Dong, W., Watson, A.M., and Hong, Y. (2009). From the  
572 Cover: Directed, efficient, and versatile modifications of the *Drosophila* genome by  
573 genomic engineering. *Proc. Natl. Acad. Sci. U.S.A.* *106*, 8284–8289.
- 574 Igaki, T. (2002). Eiger, a TNF superfamily ligand that triggers the *Drosophila* JNK  
575 pathway. *Embo J.* *21*, 3009–3018.
- 576 Iwai, Y., Usui, T., Hirano, S., Steward, R., Takeichi, M., and Uemura, T. (1997).  
577 Axon patterning requires DN-cadherin, a novel neuronal adhesion receptor, in the  
578 *Drosophila* embryonic CNS. *Neuron* *19*, 77–89.
- 579 Jo, J., Im, S.H., Babcock, D.T., Iyer, S.C., Gunawan, F., Cox, D.N., and Galko, M.J.  
580 (2017). *Drosophila* caspase activity is required independently of apoptosis to produce  
581 active TNF/Eiger during nociceptive sensitization. *Cell Death Dis* *8*, e2786.

- 582 Kaibuchi, K., Kuroda, S., and Amano, M. (1999). Regulation of the cytoskeleton and  
583 cell adhesion by the Rho family GTPases in mammalian cells. *Annu. Rev. Biochem.*  
584 *68*, 459–486.
- 585 Kanda, H., Igaki, T., Kanuka, H., Yagi, T., and Miura, M. (2002). Wengen, a member  
586 of the *Drosophila* tumor necrosis factor receptor superfamily, is required for Eiger  
587 signaling. *J. Biol. Chem.* *277*, 28372–28375.
- 588 Kauppila, S., Maaty, W.S.A., Chen, P., Tomar, R.S., Eby, M.T., Chapo, J., Chew, S.,  
589 Rathore, N., Zachariah, S., Sinha, S.K., et al. (2003). Eiger and its receptor, Wengen,  
590 comprise a TNF-like system in *Drosophila*. *Oncogene* *22*, 4860–4867.
- 591 Kimura, K., Ito, M., Amano, M., Chihara, K., Fukata, Y., Nakafuku, M., Yamamori,  
592 B., Feng, J., Nakano, T., Okawa, K., et al. (1996). Regulation of myosin phosphatase  
593 by Rho and Rho-associated kinase (Rho-kinase). *Science* *273*, 245–248.
- 594 Klapholz, B., Herbert, S.L., Wellmann, J., Johnson, R., Parsons, M., and Brown, N.H.  
595 (2015). Alternative mechanisms for talin to mediate integrin function. *Curr. Biol.* *25*,  
596 847–857.
- 597 Koenderink, G.H., Dogic, Z., Nakamura, F., Bendix, P.M., MacKintosh, F.C.,  
598 Hartwig, J.H., Stossel, T.P., and Weitz, D.A. (2009). An active biopolymer network  
599 controlled by molecular motors. *Proc. Natl. Acad. Sci. U.S.a.* *106*, 15192–15197.
- 600 Kollmannsberger, P., Mierke, C.T., and Fabry, B. (2011). Nonlinear viscoelasticity of  
601 adherent cells is controlled by cytoskeletal tension. *Soft Matter* *7*, 3127–3132.
- 602 Krens, S.F.G., Veldhuis, J.H., Barone, V., Čapek, D., Maître, J.-L., Brodland, G.W.,  
603 and Heisenberg, C.-P. (2017). Interstitial fluid osmolarity modulates the action of  
604 differential tissue surface tension in progenitor cell segregation during gastrulation.  
605 *Development* *144*, 1798–1806.
- 606 Laklai, H., Miroshnikova, Y.A., Pickup, M.W., Collisson, E.A., Kim, G.E., Barrett,  
607 A.S., Hill, R.C., Lakins, J.N., Schlaepfer, D.D., Mouw, J.K., et al. (2016). Genotype  
608 tunes pancreatic ductal adenocarcinoma tissue tension to induce matricellular fibrosis  
609 and tumor progression. *Nat Med* *22*, 497–505.
- 610 Lange, J.R., and Fabry, B. (2013). Cell and tissue mechanics in cell migration. *Exp.*  
611 *Cell Res.* *319*, 2418–2423.
- 612 Lee, A., and Treisman, J.E. (2004). Excessive Myosin activity in *mbs* mutants causes  
613 photoreceptor movement out of the *Drosophila* eye disc epithelium. *Mol. Biol. Cell*  
614 *15*, 3285–3295.
- 615 Lehmann, R., and Tautz, D. (1994). In situ hybridization to RNA. *Methods Cell Biol.*  
616 *44*, 575–598.
- 617 Lemaitre, B., and Hoffmann, J. (2007). The host defense of *Drosophila melanogaster*.  
618 *Annu. Rev. Immunol.* *25*, 697–743.
- 619 Levental, K.R., Yu, H., Kass, L., Lakins, J.N., Egeblad, M., Erler, J.T., Fong, S.F.T.,  
620 Csiszar, K., Giaccia, A., Weninger, W., et al. (2009). Matrix crosslinking forces



- 621 tumor progression by enhancing integrin signaling. *Cell* 139, 891–906.
- 622 Matsubayashi, Y., Louani, A., Dragu, A., Sánchez-Sánchez, B.J., Serna-Morales, E.,  
623 Yolland, L., Gyoergy, A., Vizcay, G., Fleck, R.A., Heddleston, J.M., et al. (2017). A  
624 Moving Source of Matrix Components Is Essential for De Novo Basement Membrane  
625 Formation. *Curr. Biol.* 27, 3526–3534.e4.
- 626 McKenzie, J.A.G. (2007). Roles of Rho/ROCK and MLCK in TNF-alpha-induced  
627 changes in endothelial morphology and permeability. *J. Cell. Physiol.* 213, 221–228.
- 628 Miroshnikova, Y.A., Mouw, J.K., Barnes, J.M., Pickup, M.W., Lakins, J.N., Kim, Y.,  
629 Lobo, K., Persson, A.I., Reis, G.F., McKnight, T.R., et al. (2016). Tissue mechanics  
630 promote IDH1-dependent HIF1 $\alpha$ -tenascin C feedback to regulate  
631 glioblastoma aggression. *Nat. Cell Biol.* 18, 1336–1345.
- 632 Montell, D.J. (2003). Border-cell migration: the race is on. *Nat. Rev. Mol. Cell Biol.*  
633 4, 13–24.
- 634 Moreno, E., Yan, M., and Basler, K. (2002). Evolution of TNF Signaling  
635 Mechanisms. *Current Biology* 12, 1263–1268.
- 636 Niederman, R., and Pollard, T.D. (1975). Human platelet myosin. II. In vitro  
637 assembly and structure of myosin filaments. *The Journal of Cell Biology* 67, 72–92.
- 638 Nourshargh, S., Hordijk, P.L., and Sixt, M. (2010). Breaching multiple barriers:  
639 leukocyte motility through venular walls and the interstitium. *Nat. Rev. Mol. Cell*  
640 *Biol.* 11, 366–378.
- 641 Oda, H., Uemura, T., Harada, Y., Iwai, Y., and Takeichi, M. (1994). A *Drosophila*  
642 homolog of cadherin associated with armadillo and essential for embryonic cell-cell  
643 adhesion. *Dev. Biol.* 165, 716–726.
- 644 Ohsawa, S., Sugimura, K., Takino, K., Xu, T., Miyawaki, A., and Igaki, T. (2011).  
645 Elimination of oncogenic neighbors by JNK-mediated engulfment in *Drosophila*.  
646 *Dev. Cell* 20, 315–328.
- 647 Parisi, F., Stefanatos, R.K., Strathdee, K., Yu, Y., and Vidal, M. (2014). Transformed  
648 epithelia trigger non-tissue-autonomous tumor suppressor response by adipocytes via  
649 activation of Toll and Eiger/TNF signaling. *Cell Rep* 6, 855–867.
- 650 Pelham, R.J., and Wang, Y.L. (1997). Cell locomotion and focal adhesions are  
651 regulated by substrate flexibility. *Proc. Natl. Acad. Sci. U.S.A.* 94, 13661–13665.
- 652 Ratheesh, A., Belyaeva, V., and Siekhaus, D.E. (2015). *Drosophila* immune cell  
653 migration and adhesion during embryonic development and larval immune responses.  
654 *Curr. Opin. Cell Biol.* 36, 71–79.
- 655 Reymond, N., d'Água, B.B., and Ridley, A.J. (2013). Crossing the endothelial barrier  
656 during metastasis. *Nat. Rev. Cancer* 13, 858–870.
- 657 Saez, A., Buguin, A., Silberzan, P., and Ladoux, B. (2005). Is the mechanical activity  
658 of epithelial cells controlled by deformations or forces? *Biophys. J.* 89, L52–L54.

- 659 Sata, M. (1998). TNFalpha regulation of Fas ligand expression on the vascular  
660 endothelium modulates leukocyte extravasation. *Nat Med* 4, 415–420.
- 661 Schneider, D.S., Ayres, J.S., Brandt, S.M., Costa, A., Dionne, M.S., Gordon, M.D.,  
662 Mabery, E.M., Moule, M.G., Pham, L.N., and Shirasu-Hiza, M.M. (2007). *Drosophila*  
663 *eiger* mutants are sensitive to extracellular pathogens. *PLoS Pathog.* 3, e41.
- 664 Schneider, M., Khalil, A.A., Poulton, J., Castillejo-Lopez, C., Egger-Adam, D.,  
665 Wodarz, A., Deng, W.-M., and Baumgartner, S. (2006). Perlecan and Dystroglycan  
666 act at the basal side of the *Drosophila* follicular epithelium to maintain epithelial  
667 organization. *Development* 133, 3805–3815.
- 668 Seifert, J.R.K., and Lehmann, R. (2012). *Drosophila* primordial germ cell migration  
669 requires epithelial remodeling of the endoderm. *Development* 139, 2101–2106.
- 670 Sen, A., Nagy-Zsvér-Vadas, Z., and Krahn, M.P. (2012). *Drosophila* PATJ supports  
671 adherens junction stability by modulating Myosin light chain activity. *The Journal of*  
672 *Cell Biology* 199, 685–698.
- 673 Sen, A., Sun, R., and Krahn, M.P. (2015). Localization and Function of Pals1-  
674 associated Tight Junction Protein in *Drosophila* Is Regulated by Two Distinct Apical  
675 Complexes. *J. Biol. Chem.* 290, 13224–13233.
- 676 Siekhaus, D., Haesemeyer, M., Moffitt, O., and Lehmann, R. (2010). RhoL controls  
677 invasion and Rap1 localization during immune cell transmigration in *Drosophila*. *Nat.*  
678 *Cell Biol.* 12, 605–610.
- 679 Smutny, M., Ákos, Z., Grigolon, S., Shamipour, S., Ruprecht, V., Čapek, D., Behrndt,  
680 M., Papusheva, E., Tada, M., Hof, B., et al. (2017). Friction forces position the neural  
681 anlage. *Nat. Cell Biol.* 19, 306–317.
- 682 Smutny, M., Behrndt, M., Campinho, P., Ruprecht, V., and Heisenberg, C.-P. (2015).  
683 UV laser ablation to measure cell and tissue-generated forces in the zebrafish embryo  
684 in vivo and ex vivo. *Methods Mol. Biol.* 1189, 219–235.
- 685 Smutny, M., Cox, H.L., Leerberg, J.M., Kovacs, E.M., Conti, M.A., Ferguson, C.,  
686 Hamilton, N.A., Parton, R.G., Adelstein, R.S., and Yap, A.S. (2010). Myosin II  
687 isoforms identify distinct functional modules that support integrity of the epithelial  
688 zonula adherens. *Nat. Cell Biol.* 12, 696–702.
- 689 Tepass, U., and Knust, E. (1993). Crumbs and stardust act in a genetic pathway that  
690 controls the organization of epithelia in *Drosophila melanogaster*. *Dev. Biol.* 159,  
691 311–326.
- 692 Vestweber, D. (2015). How leukocytes cross the vascular endothelium. *Nat. Rev.*  
693 *Immunol.* 15, 692–704.
- 694 Wang, N., Tolić-Nørrelykke, I.M., Chen, J., Mijailovich, S.M., Butler, J.P., Fredberg,  
695 J.J., and Stamenović, D. (2002). Cell prestress. I. Stiffness and prestress are closely  
696 associated in adherent contractile cells. *Am. J. Physiol., Cell Physiol.* 282, C606–  
697 C616.

698 Weavers, H., Evans, I.R., Martin, P., and Wood, W. (2016). Corpse Engulfment  
699 Generates a Molecular Memory that Primes the Macrophage Inflammatory Response.  
700 *Cell* 165, 1658–1671.

701 Zhang, L., and Ward, R.E. (2011). Distinct tissue distributions and subcellular  
702 localizations of differently phosphorylated forms of the myosin regulatory light chain  
703 in *Drosophila*. *Gene Expr. Patterns* 11, 93–104.

704

## 705 **Figure Legends**

706 **Figure 1. Macrophages invade the germband at the interface between the**  
707 **ectoderm and mesoderm**

708 (A) Cartoon showing the 3 pre-determined routes of macrophage migration in the  
709 embryo at Stage 12. Blue arrow marks the migration towards the amnioserosa (AS,  
710 blue) and the germband. Pink arrow indicates migration along the dorsal vessel and  
711 the brown arrow delineates the migration along the ventral nerve cord (vnc).

712 (B) Schematic of the region of the germband from a Stage 11 embryo imaged in C.

713 (C) Stills from two-photon time-lapse imaging of a Stage 11 *e22c-GAL4 srpHemo-*  
714 *3xmCherry; 10xUAS-CD8::GFP* embryo in which *CD8::GFP* labels germband  
715 membranes (green) and *srpHemo-3XmCherry* labels macrophages (red). The white  
716 arrow pinpoints the initial protrusion of the macrophage between the ectoderm and  
717 the mesoderm and the yellow arrow specifies the macrophages that migrate into the  
718 amnioserosa at 10 min. The white arrowhead indicates a gap appearing between the  
719 ectoderm and mesoderm once the macrophage penetrates the germband at 15 min. See  
720 also Movie S1 and Figure S1.

721 (D) Confocal images of fixed lateral Stage 10 and 12 wild type embryos with  
722 macrophages visualized by *srpHemo-3XmCherry* expression (red), ectoderm by  
723 antibody staining against DE-Cadherin (green) and mesoderm by antibody staining  
724 against DN-Cadherin (magenta), along with a merge of all channels. The dotted white  
725 line in the green channel indicates the apical side of the ectoderm cells.

726 (E) A magnification of the area outlined by the dotted box in D. Arrows indicate the  
727 interface of the ectoderm and mesoderm in Stage 11 embryos prior to macrophage  
728 migration when the tissues are closely apposed. Arrowheads in Stage 12 identify  
729 macrophages sitting between the two tissues that have separated.

730 (F) Schematic denoting with a blue box the region of the germband shown in (G, H)  
731 in an early Stage 10 embryo. The black dotted line within the germband in the  
732 schematic indicates the ectoderm-mesoderm interface.

733 (G) Transmission electron microscopy (TEM) image of the ectoderm-mesoderm  
734 tissue interface from an early embryo in which the macrophages have not yet reached  
735 the germband (overview in Figure S1D).

736 (H) A magnification of the area within the dotted box in G, showing that the cells at  
737 the interface are in close contact before macrophage entry into the germband (yellow  
738 arrow) with some extracellular spaces (blue arrowheads). Mesoderm cells are pseudo-  
739 colored in magenta. See also Figure S1.

740 (I, J) Confocal microscopy images of a fixed lateral Stage 11 embryo stained with an  
741 antibody against Laminin A (LanA), with macrophages visualized by *srpHemo-*  
742 *H2A::3XmCherry* and a magnification of the area indicated in dotted box in I shown  
743 in J. LanA is expressed by the mesoderm in the germband before macrophage entry.  
744 Arrowhead indicates the LanA found where the macrophages traverse into the  
745 germband, at the interface between the ectoderm and the mesoderm.

746 (K) Schematics of Stage 10 and Stage 12 embryos (grey) with box indicating the  
747 region magnified below to illustrate the morphology of the germband before (Stage  
748 10) and after (Stage 12) macrophage invasion. Macrophages (red) enter between the  
749 caudal ectoderm (green), and the visceral mesoderm (magenta) along a track of

750 Laminin A (orange). The amnioserosa adjacent to the ectoderm is in blue and the yolk  
751 in grey. See also Figure S1.

752 Embryo pictures throughout are shown with anterior to the left and dorsal up.  
753 Embryos which displayed stomodeum invagination and a germband retraction away  
754 from the anterior of less than 29%, were classified as Stage 10 and embryos with  
755 germband retractions between 29-31% for Stage 11 and 35-40% as Stage 12.

756 Scale bar represents 40 $\mu$ m in C, 20 $\mu$ m in D, I, 10 $\mu$ m in E, J, 5 $\mu$ m in G and 2 $\mu$ m in  
757 H.

758 **Figure 2. Amnioserosal Eiger (Dm-TNF) regulates macrophage invasion of the**  
759 **embryonic germband**

760 (A) *In situ* hybridizations of lateral Stage 11 embryos reveal *eiger* expression in the  
761 amnioserosa (arrow) and neural ectoderm in wild type embryos and its absence in  
762 *egr<sup>1</sup>* mutant embryos.

763 (B) Confocal microscopy images of z-projections of fixed lateral Stage 12 embryos,  
764 stained with DE-Cadherin antibody (green). Control (con) and *egr<sup>1</sup>* mutant embryos  
765 are shown, with macrophages labeled in red by the expression of  
766 *srpHemo>H2A::RFP*. The dotted line demarcates the edge of the germband. Arrows  
767 in *egr<sup>1</sup>* indicate accumulation of macrophages outside the germband.

768 (C) Schematic drawing of a lateral Stage 12 embryo depicting the paths taken by  
769 macrophages (red dots) migrating into the germband. The blue circle indicates the  
770 area analyzed to count the number of macrophages in the germband throughout the  
771 manuscript.

772 (D) Quantification reveals that the number of macrophages that have moved into the  
773 germband in Stage 12 is decreased in embryos from *egr<sup>1</sup>*, *egr<sup>3</sup>*, and

774 *egr<sup>l</sup>/Df(2R)BSC303* which removes *egr* completely. Macrophages were labeled by the  
775 expression of *srpHemo>H2A::RFP*. n=20 embryos for each genotype.

776 **(E)** Quantification of macrophages in the germband in embryos from the control  
777 (con), the *egr<sup>l</sup>* mutant, and the *egr<sup>l</sup>* mutant expressing *UAS-eiger* under the control of  
778 the LP1 amnioserosal GAL4 driver which was able to partially rescue the mutant  
779 phenotype. n=25 embryos for all genotypes. See also Figure S2.

780 **(F)** Quantification of the number of macrophages that have penetrated the germband  
781 in Stage 12 embryos in control (con) embryos and those in which an amnioserosal  
782 (*c381-GAL4*) driver directs the expression of an RNAi against *eiger*. n=20 embryos  
783 for all genotypes. See also Figure S2.

784 **(G)** Schematic drawing of the anterior half of a lateral Stage 11 embryo indicating the  
785 region analyzed (area within blue box) to quantify the **(H)** speed and **(I)** persistence of  
786 macrophage migration up to the germband in two-photon movies from wild type and  
787 *egr<sup>l</sup>* mutant embryos with macrophage nuclei labeled with *srpHemo-*  
788 *H2A::3xmCherry*. Speed was unaffected and persistence was mildly reduced. n=3  
789 embryos for each genotype. See also Figure S2 and Movies S2 and S3.

790 **(J)** Stills from two-photon movies of control (con) *srpHemo-H2A::3xmCherry* and  
791 *egr<sup>l</sup>; srpHemo-H2A::3xmCherry* embryos showing macrophage nuclei migrating  
792 from the head into the germband at the indicated time points. The white dotted line  
793 indicates the edge of the germband that was detected using autofluorescence from the  
794 yolk. Movie areas (Movie S2) correspond to the dashed box in the schematic embryos  
795 above. See also Figure S2 and Movies S2 and S3.

796 **(K)** Left: Schematic showing the entry of the first macrophage into the germband  
797 (green arrow). Amnioserosa (AS) indicated in blue. The time required for macrophage  
798 entry after first contact with the germband is quantified and is significantly increased

799 in *egr<sup>1</sup>* mutants compared to the control (con). Macrophages were labeled with  
800 *srpHemo::3xmCherry* and the germband with *knock-in DE-Cad::GFP*. n=5 embryos  
801 for both genotypes.

802 (L) Schematic indicating the regions of the germband in which migration of the first  
803 macrophage was quantified in M and N. (M) Migration within the region of the  
804 germband adjacent to the AS (light blue), shown with a dark blue arrow, is  
805 significantly lower whereas (N) further migration along the germband (brown arrow)  
806 is not significantly altered. n=3 embryos for both genotypes. See also Figure S2.

807 Histograms show mean  $\pm$  s.e.m. \*\*\*P<0.001, \*\*P<0.01, ns not significant. One-way  
808 ANOVA with Dunnett post test used for D,F,H,I and One-way ANOVA with Tukey  
809 for E, unpaired t-test for K,M,N.

810 All embryos are oriented with anterior to the left and dorsal up, unless otherwise  
811 noted. The black dotted line within the germband in the schematics shown in C,J,K,L  
812 indicate the ectoderm-mesoderm interface. Embryos were staged for imaging and  
813 quantification based on having germband retraction away from the anterior of 29-31%  
814 for Stage 11 and 35-40% for Stage 12. Scale bar represents 50 $\mu$ m in A,B and 40 $\mu$ m in  
815 J.

816

817 **Figure 3. Grindelwald (Dm-TNFR) expressed in the ectoderm is essential for**  
818 **macrophage germband invasion**

819 Confocal images of a single sagittal section of (A) a lateral wild type Stage 10 and (B)  
820 a Stage 11 embryo with macrophage nuclei labeled by the expression of *srpHemo-*  
821 *H2A::3XmCherry* (red) and Eiger recognized with an antibody (green). The regions  
822 imaged in A and B correspond to the magnified areas of the grey embryo depicted in  
823 the adjoining schematics on the left, in which macrophages are shown in red and the

824 amnioserosa (AS) in blue. The black dotted line within the germband in the  
825 schematics indicates the ectoderm-mesoderm interface. (**A'**, **B'**) Right panels show a  
826 magnification of the area indicated by the white dotted box in the adjoining panels on  
827 the left. (**A'**) We observe punctate membrane expression of Eiger in AS cells in Stage  
828 10 (arrowhead) and almost no localization in the germband ectoderm (arrow). (**B'**) In  
829 Stage 11 before the macrophages enter the germband we observe some Eiger  
830 remaining on the AS (also see Figure S3B,B') but also additional localization on the  
831 germband ectoderm (arrow in **B'**).

832 (**C, D**) Quantification in Stage 10 and 11 embryos of the intensity of Eiger antibody  
833 staining at the membrane normalized to the cytoplasm in the (**C**) AS and (**D**)  
834 ectoderm. n=30 cell boundaries, 5 embryos for each genotype. See also Figure S3.

835 (**E**) *In situ* hybridizations of Stage 11 embryos reveal that in wild type *grindelwald* is  
836 expressed in the ectoderm, particularly highly in the germband (arrowhead), and that  
837 *grnd*<sup>Minos</sup> embryos show no expression.

838 (**F**) Confocal microscopy images of z-projections of fixed lateral Stage 12 embryos,  
839 from the control (con) and a line in which RNAi against *grindelwald* is driven by the  
840 *e22c-GAL4* ectodermal driver. Macrophages are labeled in red by the expression of  
841 *srpHemo:3xmCherry*. The white dotted line indicates the edge of the germband.  
842 Quantification on the right shows that RNAi knockdown of *grindelwald* in the  
843 ectoderm results in reduced macrophage entry into the germband. n=22 embryos for  
844 both genotypes.

845 (**G**) Confocal microscopy images of z-projections of fixed lateral Stage 12 embryos.  
846 Control (con) and *grnd*<sup>Minos</sup> mutant embryos are shown, with macrophages labeled in  
847 red by the expression of *srpHemo-H2A::3xmCherry*. The dotted line demarcates the



848 edge of the germband. Quantification shows that the *grind*<sup>Minos</sup> mutant displays  
849 reduced macrophage entry into the germband. n=17 embryos for both genotypes.

850 (H) Stills from two-photon movie of *grnd*<sup>Minos</sup>; *srpHemo-H2A::3xmCherry* embryo  
851 showing macrophage nuclei migrating from head into the germband at the indicated  
852 time points. The white dotted line indicates the edge of the germband, which was  
853 detected using autofluorescence from the yolk. The region imaged in the movie  
854 (Movie S2) corresponds to the dashed boxed area in the schematic embryos above.  
855 See also Figure S3 and Movies S2 and S3.

856

857 Histograms show mean  $\pm$  s.e.m. Unpaired t-test in **C,D,F,G**. \*\*\*\*P<0.0001.

858 The black dotted line within the germband in the schematics indicates the ectoderm-  
859 mesoderm interface. Embryos shown with anterior to left and dorsal up in all panels.  
860 Embryos were staged for imaging and quantification based on germband retraction  
861 away from the anterior of less than 29% for Stage 10, 29-31% for Stage 11 and 35-  
862 40% for Stage 12. Scale bars represent 10 $\mu$ m in **A-B'**, 40 $\mu$ m in **H** and 50 $\mu$ m in  
863 **E,F,G**.

864

865 **Figure 4: Eiger (Dm-TNF) does not regulate adhesion at the ectoderm-mesoderm**  
866 **interface.**

867 (A) Schematic drawings of a lateral Stage 11 embryo (grey, on top) and a  
868 magnification of the region near the germband (in dotted box, middle) depicting  
869 macrophages in red at the edge of the germband prior to entry. The black dotted line  
870 within the germband section highlighted in the small dotted box indicates the  
871 ectoderm-mesoderm interface. Below is a schematic indicating the arrangement of

872 the ectoderm (green) and mesoderm (magenta) cells in the germband. Blue box in the  
873 lowest schematic indicates the region shown in **B, E-G**.

874 (**B,E-G**) Confocal microscopy images of a single sagittal plane at the ectoderm-  
875 mesoderm interface (blue box in **A**) from control (con) and *egr<sup>1</sup>* mutant embryos with  
876 *srpHemo-H2A::3xmCherry* in the background to label macrophage nuclei. Stage 11  
877 embryos were selected for imaging and quantification based on having germband  
878 retraction away from the anterior of 29-31% and macrophages at or near the edge of  
879 the germband. Embryos were imaged with antibodies against (**B**) DE-Cadherin  
880 (green) and N-Cadherin (magenta), (**E**) Dystroglycan (green), (**F**) DE-Cadherin  
881 (green) and  $\beta$ -PS integrin or (**G**) Talin shown in magenta. The white dotted line in the  
882 left panel indicates the ectoderm-mesoderm interface. See also Figure S4.

883 (**C,D,H-K**) Quantification of the interface intensity, normalized to cytoplasmic  
884 background, of (**C**) DE-Cadherin, (**D**) N-Cadherin, (**H**) Laminin A, (**I**) Dystroglycan,  
885 (**J**)  $\beta$ -PS integrin, and (**K**) Talin in control (con) and *egr<sup>1</sup>* mutant embryos. See also  
886 Figure S4.

887 Anterior to left and dorsal up in all panels. Scale bars represent 10 $\mu$ m. Histograms  
888 show mean  $\pm$  s.e.m. ns = not significant, unpaired t-test.

889

890 **Figure 5: Eiger (Dm-TNF) supports apical Patj localization and regulates myosin**  
891 **activity in the germband ectoderm.**

892 (**A**) Quantification of apoptotic corpses, labeled with an antibody against activated  
893 Caspase 3, in the germband of Stage 12 shows no significant difference between  
894 control (con), *egr<sup>1</sup>* and *grnd<sup>Minos</sup>* embryos expressing *srpHemo-H2A::3xmCherry* to  
895 label macrophages. n=15 embryos for all genotypes. See also Figure S5.

896 **(B)** Confocal microscopy images of z-projections of fixed lateral Stage 12 embryos  
897 from control (con) embryos and those in which RNAi against *veli* is driven by the  
898 *e22c-GAL4* ectodermal driver. Macrophages are labeled in red by the expression of  
899 *srpHemo:3xmCherry*. The white dotted line indicates the edge of the germband.  
900 Quantification reveals that RNAi knockdown of *veli* in the ectoderm leads to a strong  
901 reduction in macrophage invasion into the germband. n=25 embryos for both  
902 genotypes.

903 **(C)** Schematics showing a Stage 12 embryo with the region boxed represented in the  
904 lower schematic, in which the black dotted line within the germband delineates the  
905 ectoderm-mesoderm interface. The blue box indicates the region of the germband  
906 imaged and analyzed in **D-I**.

907 **(D,F,H)** Confocal images of the germband ectoderm (blue boxed area in lower  
908 schematic in **C**) from fixed lateral Stage 12 embryos in which macrophages were at or  
909 near the edge of the germband. Control (con), *egr<sup>l</sup>* and *grnd<sup>Minos</sup>* embryos were  
910 immunolabeled for **(D)** Crumbs, **(F)** Patj, or **(H)** the phosphorylated form of Myosin  
911 Regulatory Light Chain, p-MRLC, also called Sqh-1P. See also Figure S5.

912 **(E,G,I)** Quantification of line scan analysis of apical Crumbs, Patj and Sqh-1P levels  
913 normalized to their respective cytoplasmic level. **(E)** Crumbs was not significantly  
914 altered, but **(G)** apical Patj levels were significantly lower, and **(I)** Sqh-1P levels were  
915 significantly higher in the *egr<sup>l</sup>* and *grnd<sup>Minos</sup>* embryos compared to the control (con).  
916 n=6 embryos and 30 contacts of each genotype for Crumbs analysis, 7 and 37 for Patj  
917 and 7 and 40 for Sqh-1P.

918 **(J)** Confocal microscopy images of z-projections of fixed lateral Stage 12 embryos  
919 from the control (con), the *egr<sup>l</sup>* mutant, and the *egr<sup>l</sup>* mutant expressing *UAS-Patj* or  
920 an RNAi against MRLC (*sqh*) under the control of the *e22c-GAL4* ectodermal driver.

921 Macrophages were labeled in red by the expression of *srpHemo-H2A::3xmCherry*.  
922 The white dotted line indicates the edge of the germband.  
923 **(K)** Quantification indicates that expression of *patj* or removal of MRLC in the  
924 ectoderm as described in **J** partially rescues the *egr<sup>1</sup>* mutant phenotype. n=20 embryos  
925 for control, *egr<sup>1</sup>* and *patj* rescue. n=18 embryos for *MRLC* knockdown.  
926 Embryos were staged for quantification and imaging based on having germband  
927 retraction away from the anterior of 29-31% for Stage 11 and 35-40% for Stage 12.  
928 Anterior to left and dorsal up in all panels. Scale bar represents 50µm in **B,J** and  
929 10µm in **D,F,H**. \*\*\*\*P<0.0001, \*\*\*P<0.001, ns=not significant. One-way ANOVA  
930 with Dunnett post test for **A,E,G,I**. One-way ANOVA with Tukey for **K** and unpaired  
931 t-test for **B**.

932

### 933 **Figure 6: Eiger regulates apical tension in the germband ectoderm**

934 **(A)** Schematic drawing (left panel) of a dorsal Stage 11 embryo indicating the  
935 ectodermal region where laser ablation was conducted (green box). Schematic (right  
936 panel) depicting single cell ablation showing a line (red) cut perpendicular to the  
937 apical DE-Cadherin (light blue) and centered between neighboring cell vertexes.  
938 Displacement of apical DE-Cadherin after severing is indicated (black arrows).

939 **(B)** Stills from confocal spinning disc movies (left panel) showing ectodermal apical  
940 DE-Cadherin::GFP in control, *egr<sup>1</sup>* and *grnd<sup>Minos</sup>* embryos before (precut) and 1 sec  
941 (s) after laser ablation (postcut). Embryos where macrophages were near or at the  
942 edge of but not within the germband were chosen for ablations. Area of ablated DE-  
943 Cadherin::GFP along the apical cell cortex is indicated (red arrow) and outer edges  
944 for kymograph analysis in **C** are marked (light blue arrowheads). See also Figure S6  
945 and Movie S5.

946 (C) Kymograph analysis showing apical DE-Cadherin::GFP before (pre), during (red  
947 arrow) and after laser ablation (postcut) in control, *egr<sup>l</sup>* and *grnd<sup>Minos</sup>* embryos. Black  
948 arrows indicate the time (s) after ablation. The open-ends of the gap left after severing  
949 DE-Cadherin::GFP are highlighted with green lines to illustrate retraction behavior.

950 (D) Displacement of the apical cell cortex labeled with DE-Cadherin::GFP is shown  
951 for each 800ms time frame post-cut and the values were curve fitted using  
952 nonparametric fitting with smoothing splines. Time resolved displacement is higher  
953 after the cut in *egr<sup>l</sup>* and *grnd<sup>Minos</sup>* embryos as compared to control, indicating greater  
954 tension.

955 (E) *egr<sup>l</sup>* and *grnd<sup>Minos</sup>* embryos when compared to control show an increased initial  
956 recoil velocity after the cut of the apical cell cortex labeled with DE-Cadherin::GFP.  
957 n=20 embryos for control, 15 for *egr<sup>l</sup>*, and 8 for *grnd<sup>Minos</sup>*.

958 (F) Recoil velocity is lower in control (con) and *egr<sup>l</sup>* embryos when injected with the  
959 Rho Kinase inhibitor drug Y27632 (+Y) compared to uninjected control embryos.  
960 n=20 embryos for control, 12 for control + Y27632, 15 for *egr<sup>l</sup>*, and 7 for *egr<sup>l</sup>* +  
961 Y27632.

962 (G) Quantification reveals a decrease in the number of macrophages that have  
963 migrated into the germband in Stage 12 embryos expressing a dominant active form  
964 of Rho1 (*UAS-Rho1.V14*) in the ectoderm under the control of the *e22c-GAL4*  
965 ectodermal driver compared to the control (con). Embryos were staged for  
966 quantification and imaging based on having germband retraction away from the  
967 anterior of 35-40% for Stage 12. n=20 embryos for both genotypes. See also Figure  
968 S6.

969 (H) Left: Schematic showing a Stage 12 embryo viewed dorsally. The ectodermal  
970 cells in the green boxed area are shown magnified below at time point 0 when the

971 macrophage protrusion touches the basal side of the ectoderm cells and time point 3  
972 when the macrophage has fully insinuated itself under the ectoderm. Right:  
973 Quantification of two-photon movies of the ectodermal cell deformations that occur  
974 during macrophage migration into the area of the germband shown in the green box in  
975 the schematic. Ectoderm visualized with *knock-in DE-CAD::GFP* and macrophages  
976 visualized with *srpHemo-3xmCherry* in wild type and *egr<sup>l</sup>* mutant embryos.  
977 Deformations are measured only for ectodermal cells within a 10 $\mu$ m radius of the  
978 macrophage cell edge. The length/ width ratio (LWR) of the ectodermal cells, shown  
979 on the y-axis is plotted over time, indicated on the x-axis. Time interval 40 seconds,  
980 n=3 embryos for each genotype, 10-40 cells for each time point. See also Figure S6  
981 and Movie S7.

982 **(I)** Model: Eiger binding to the Grindelwald receptor results in greater localization of  
983 Patj and its binding partner, the Myosin phosphatase, MBS. This leads to a decrease  
984 in the level of active phosphorylated Myosin, and lower ectodermal apical tension,  
985 which facilitates macrophage invasion into the germband.

986 Anterior to left and dorsal up in all panels. Scale bar in **B** represents 10 $\mu$ m. Anterior  
987 to left in all panels. \*\*\*P<0.001, \*\*P<0.01, \* P<0.05. One-way ANOVA with  
988 Dunnett post test for **G**. Unpaired t-test for **E,F,H**.

989

990

991

992

993

994

995

996 **STAR Methods**

997 **CONTACT FOR REAGENT AND RESOURCE SHARING**

998 Further information and requests for resources and reagents should be directed to and  
999 will be fulfilled by the Lead Contact, Dr. Daria Siekhaus ([daria.siekhaus@ist.ac.at](mailto:daria.siekhaus@ist.ac.at)).

1000 **EXPERIMENTAL MODEL AND SUBJECT DETAILS**

1001 **Fly strains and preparation**

1002 Flies were raised on standard food bought from IMBA (Vienna, Austria) which  
1003 contained agar, cornmeal, and molasses with the addition of 1.5% Nipagin. Adults  
1004 were placed in cages in a Percival DR36VL incubator maintained at 25°C and 65%  
1005 humidity; embryos were collected on standard plates prepared in house from apple  
1006 juice, sugar, agar and Nipagin supplemented with yeast from Lesaffre (Marcq,  
1007 France) on the plate surface. Fly crosses and embryo collections for RNA interference  
1008 experiments (7 hour collection) as well as live imaging (6 hour collection) were  
1009 conducted at 29°C. All fly lines utilized are listed below: *srpHemo-GAL4* was  
1010 provided by K. Brückner (UCSF, USA) (Brückner et al., 2004) and *egr<sup>1</sup>*, *egr<sup>3</sup>*, *UAS-*  
1011 *egr* (weak) and *UAS-egr IR* lines were provided by M. Galko (MD Anderson Cancer  
1012 Centre, USA) and have been previously described (Igaki, 2002). The *knock-in DE-*  
1013 *Cad::GFP* line which contains GFP fused to the C terminus of Cadherin and knocked  
1014 into the endogenous locus was provided by Y. Hong (Huang et al., 2009). *grnd<sup>Minos</sup>*  
1015 and *UAS-grnd IR* lines were provided by P. Leopold (iBV, France) and have been  
1016 previously described (Andersen et al., 2015). *Puc<sup>E69</sup>-GAL4* was provided by A.  
1017 Classen (University of Munich, Germany). *srpHemo-H2A::3xmCherry* and *srpHemo-*  
1018 *3xmCherry* lines have been previously described (Gyoergy et al., 2018). The  
1019 following lines were obtained from the Bloomington Stock Centre: *UAS-Patj*  
1020 (BL39735), *UAS-sqh* RNAi line (TRiP HMS00437), *Df(2R)BSC303*, *10xUAS-*

1021 *CD8::GFP*, *c381-GAL4*, *sg3-GAL4*, *LPI-GAL4*, *e22c-GAL4* and *UAS-Rho.V14*. The  
1022 *UAS-grnd* RNAi line KK104538 was obtained from the Vienna Drosophila Resource  
1023 Center (VDRC), Vienna, Austria.

#### 1024 **Embryo staging**

1025 Fixed embryos which had completed germband extension were staged for imaging  
1026 based on the invagination of the stomodeum as well as germband retraction away  
1027 from the anterior. Embryos which showed stomodeum invagination and a germband  
1028 retraction of less than 29% was classified as Stage 10 and embryos with germband  
1029 retractions between 29-31% for Stage 11 and 35-40% for Stage 12.

#### 1030 **The lines used in each Figure are listed below**

1031 **Figure 1C:** *e22c-GAL4 srp-3xmCherry*; *10xUAS-CD8::GFP*. **Figure 1D,E,G,H** and  
1032 **Figure S1D,E:** +; *srpHemo-3xmCherry*. **Figure 1I,J:** +; *srpHemo-H2A::3xmCherry*.

1033 **Figure 2A** and **Figure S2B,C**, *Oregon R*, *egr<sup>1</sup>*. **Figure 2B** and **Figure S2A, F-K:** +;  
1034 *srpHemo-GAL4 UAS-GFP UAS-H2A::RFP*, *egr<sup>1</sup>*; *srpHemo-GAL4 UAS-GFP UAS-*  
1035 *H2A::RFP*. **Figure 2D:** +; *srpHemo-GAL4 UAS-GFP UAS-H2A::RFP*, *egr<sup>1</sup>*;  
1036 *srpHemo-GAL4 UAS-GFP UAS-H2A::RFP*, *egr<sup>3</sup>*; *srpHemo-GAL4 UAS-GFP UAS-*  
1037 *H2A::RFP*, *Df(2R)BSC303/ egr<sup>1</sup>*; *srpHemo-GAL4 UAS-GFP UAS-H2A::RFP*. **Figure**  
1038 **2E** and **Figure S2D:** +; *srpHemo-3xmCherry*, *egr<sup>1</sup>*; *srpHemo-3xmCherry*, *egr<sup>1</sup> UAS-*  
1039 *egr*; *LPI-GAL4 srpHemo-3xmCherry*. **Figure 2F** and **Figure S2E:** +; *srpHemo-*  
1040 *3xmCherry/+*, *UAS-egr IR/+*; *srpHemo-3xmCherry/+*; *c381-GAL4/+*. **Figure**  
1041 **2H,LM,N**, **Figure S2M,O:** +; *srpHemo-H2A::3xmCherry*, *egr<sup>1</sup>*; *srpHemo-*  
1042 *H2A::3xmCherry*. **Figure 2K:** knock-in *DE-Cad::GFP srpHemo-3xmCherry*, *egr<sup>1</sup>*  
1043 knock-in *DE-Cad::GFP srpHemo-3xmCherry*.



1044 **Figure 3A,A',B,B',C,D and Figure S3A,A',B,B'**: +; *srpHemo-H2A::3xmCherry*.

1045 **Figure 3E: Oregon R, *grnd*<sup>Minos</sup>**. **Figure 3F: *e22c-GAL4, srpHemo-3xmCherry; UAS-***

1046 ***GFP, e22c-GAL4, srpHemo-3xmCherry; UAS-grnd RNAi KK***. **Figure 3G,H and**

1047 **Figure S3C,E-I: +; *srpHemo-H2A::3xmCherry, grnd*<sup>Minos</sup>; *srpHemo-***

1048 ***H2A::3xmCherry***.

1049 **Figure 4B,C,D,H and Figure S4A-E,M: *srpHemo-H2A::3xmCherry, egr*<sup>1</sup>; *srpHemo-***

1050 ***H2A-3xmCherry***. **Figure 4 E,F,G,I,J,K and Figure S4 F-K: *srpHemo-***

1051 ***H2A::3xmCherry, egr*<sup>1</sup>; *srpHemo-H2A::3xmCherry***.

1052 **Figure 5A,D,E Figure S5A,D (Crumbs immunolabeling): +; *srpHemo-***

1053 ***H2A::3xmCherry, egr*<sup>1</sup>; *srpHemo--H2A::3xmCherry, grnd*<sup>Minos</sup>; *srpHemo-***

1054 ***H2A::3xmCherry***. **Figure 5B: *e22c-GAL4 srpHemo-3xmCherry; UAS-GFP, e22c-***

1055 ***GAL4 srpHemo-3xmCherry; UAS-veli IR***. **Figure 5F-I and Figure S5D (Patj and**

1056 **Sqh-1P immunolabeling): +; *srpHemo-H2A::3xmCherry, egr*<sup>1</sup>; *srpHemo-***

1057 ***3xmCherry, grnd*<sup>Minos</sup>; *srpHemo-3xmCherry***. **5J,K: *e22c-GAL4 srpHemo-3xmCherry;***

1058 ***UAS-GFP, e22c-GAL4 srpHemo-3xmCherry egr*<sup>1</sup>; *UAS-GFP, e22c-GAL4 srpHemo-***

1059 ***3xmCherry egr*<sup>1</sup>; *UAS-Patj, e22c-GAL4 srpHemo-3xmCherry egr*<sup>1</sup>; *UAS-sqh IR***.

1060 **Figure S5B,C: *UAS-GFP; srpHemo-3xmCherry, puc*<sup>E69</sup>-*GAL4, egr*<sup>1</sup> *UAS-GFP;***

1061 ***srpHemo-3xmCherry puc*<sup>E69</sup>-*GAL4***. **Figure S5E,F: +; *srpHemo-H2A::3xmCherry***.

1062 **Figure 6B,C,D,E and Figure S6A: *knock-in DE-Cad::GFP srpHemo-3xmCherry,***

1063 ***egr*<sup>1</sup> *DE-Cad::GFP srpHemo-3xmCherry, grnd*<sup>Minos</sup>; *knock-in DE-Cad::GFP***

1064 ***srpHemo-3xmCherry***. **Figure 6F,H and Figure S6F: *knock-in DE-Cad::GFP***

1065 ***srpHemo-3xmCherry, egr*<sup>1</sup> *knock-in DE-Cad::GFP srpHemo-3xmCherry***. **Figure 6G**

1066 **and Figure S6E: *e22c-GAL4 srpHemo-3xmCherry/+; UAS-GFP/+; e22c-GAL4***

1067 ***srpHemo-3xmCherry/+; UAS-Rho.V14/+***. **Figure S6C,D: +; *srpHemo-***

1068 ***H2A::3xmCherry, egr*<sup>1</sup>; *srpHemo-3xmCherry***.

## 1069 **METHODS DETAILS**

### 1070 **In situ hybridization and immunofluorescence**

1071 Embryos were fixed with 3.7% formaldehyde/heptane for 20 min followed by  
1072 methanol devitellinization for *in situ* hybridization. The *eiger* cDNA clone, RH51659  
1073 and the *grindelwald* cDNA clone RE28509 were obtained from the *Drosophila*  
1074 Genomics Resource Centre (DGRC). T7 or T3 polymerase-synthesized digoxigenin-  
1075 labelled anti-sense probe preparation and *in situ* hybridization was performed using  
1076 standard methods (Lehmann and Tautz, 1994). Images were taken with a Nikon-  
1077 Eclipse Wide field microscope with a 20X 0.5 NA DIC water Immersion Objective.  
1078 For most antibody stainings, embryos were fixed with freshly prepared 4.0%  
1079 paraformaldehyde and heptane for 20 min followed by methanol devitellinization as  
1080 described previously (Zhang and Ward, 2011). Phalloidin, DE-Cadherin and N-  
1081 Cadherin staining utilized hand-devitellinized embryos. Eiger staining was conducted  
1082 on embryos devitellinized with ethanol. The following primary antibodies were used.  
1083 Chicken Anti-GFP (Aves Labs GFP-1020, 1:500), Rabbit anti-E-Cadherin (Santa  
1084 Cruz sc-33743, 1:25), Rat anti-DE-Cadherin (Oda et al., 1994) (DSHB DCAD2,  
1085 1:25), Rat anti-DN-Cadherin (Iwai et al., 1997) (DSHB DN-Ex #8, 1:25), Mouse anti-  
1086 Talin (Brown et al., 2002) (DSHB Talin A22A, Talin E16B, 1:10), Mouse anti-  
1087 Integrin betaPS (Brower et al., 1984) (DSHB CF.6G11, 1:25), Mouse anti-Crumbs  
1088 (Tepass and Knust, 1993) (DSHB CQ4, 1:50), Rabbit anti-Dystroglycan (Deng et al.,  
1089 2003)1:50), Rabbit anti-LanA (Schneider et al., 2006)1:50), Rabbit Eiger R1 (Igaki,  
1090 2002), guinea pig anti-Patj (Sen et al., 2012), guinea pig anti-Sqh1P ((Zhang and  
1091 Ward, 2011). Alexa fluor 488 or 633 labelled secondary antibodies and Phalloidin  
1092 (Thermo Fisher Scientific) were used at a dilution of 1:500. Embryos were mounted  
1093 after immunolabeling in Vectashield Mounting Medium (Vector Labs, Burlingame,

1094 USA) and imaged with a Zeiss Inverted LSM700 Confocal Microscope using a Plain-  
1095 Apochromat 20X/0.8 Air Objective or a Plain-Apochromat 63X/1.4 Oil Objective as  
1096 required.

### 1097 **Electron Microscopy**

1098 Early embryos in which the macrophages had not yet reached the germband were  
1099 collected and dechorionated before mounting on cup-shaped aluminum planchettes  
1100 (cavity dimensions Ø 2mm, depth 200µm; Wohlwend, Sennwald, CH) using 2% BSA  
1101 in phosphate buffer (0.1M, pH 7.4) as filler and a flat planchette as a lid. Such  
1102 sandwiched samples were rapidly frozen using a HPF machine (HPM010; BalTec,  
1103 Balzers, LIE) and stored in liquid nitrogen. Embryos were then freeze-substituted in  
1104 an AFS1 device (Leica Microsystems) using the following FS cocktail: 1% osmium  
1105 (w/v; EMS) in non-hydrous acetone plus 0.2% uranyl acetate (v/v of 20% stock in  
1106 methanol; Agar Scientific). The sequence for step-wise warming was: -80°C for 48 h,  
1107 temperature rise 3°C/h, -20°C for 12 h, temperature rise 3°C/h, 4°C for 1 h. Embryos  
1108 were then washed in non-hydrous acetone, embedded in epoxy resin (Durcupan  
1109 ACM, Fluka) and cured for 48 h at 60°C. Serial ultrathin sections (70-80 nm) were  
1110 cut using an ultramicrotome (Leica Microsystems UC7), collected onto formvar-  
1111 coated copper slot grids and contrast enhanced by means of 1% uranyl acetate in  
1112 water (w/v) and 0.3% lead citrate. Sections were examined in a TECNAI 10  
1113 transmission electron microscope operated at 80 kV, equipped with a Morada CCD  
1114 camera (Soft Imaging Systems). Alternatively, sections were cut at 250 nm, collected  
1115 on formvar-coated 100-line bar grids, carbon coated (thickness 6 nm) and observed  
1116 under a Jeol JEM 2800 operated at 200 kV in STEM bright-field mode.

1117

### 1118 **Time-Lapse Imaging**

1119 Embryos were dechorionated in 50% bleach for 4 min, washed with water, and  
1120 mounted in halocarbon oil 27 (Sigma) between a coverslip and an oxygen permeable  
1121 membrane (YSI). The anterior dorsolateral region of the embryo was imaged on an  
1122 inverted multiphoton microscope (TrimScope II, LaVision) equipped with a W Plan-  
1123 Apochromat 40X/1.4 oil immersion objective (Olympus). GFP and mCherry were  
1124 imaged at 860 nm and 1100 nm excitation wavelengths, respectively, using a Ti-  
1125 Sapphire femtosecond laser system (Coherent Chameleon Ultra) combined with  
1126 optical parametric oscillator technology (Coherent Chameleon Compact OPO).  
1127 Excitation intensity profiles were adjusted to tissue penetration depth and Z-  
1128 sectioning for imaging was set at 1 or 1.5  $\mu\text{m}$  for tracking and segmentation  
1129 respectively. For long-term imaging, movies were acquired for 180-200 minutes with  
1130 a frame rate of 40 seconds. All embryos were imaged with a temperature control unit  
1131 set to 28.5°C. To assess potential changes in germband extension and retraction in the  
1132 *egr<sup>1</sup>* embryos, wild type and *egr<sup>1</sup>* embryos were collected for 30 minutes and then  
1133 imaged for a further 10 hours using a Nikon-Eclipse Wide field microscope with a  
1134 20X 0.5 NA DIC water Immersion Objective. Bright field images were taken every 5  
1135 minutes.

1136 **Analysis of macrophage cell counts:** Transmitted light images of the embryos were  
1137 used to measure the position of the germband to determine the stages for analysis.  
1138 Germband retraction away from the anterior was used to classify embryos into Stage  
1139 11 or Stage 12. Embryos with germband retraction of between 29-31% were assigned  
1140 to Stage 11. Those with 35-40% retraction (Stage 12) were analyzed for the number  
1141 of macrophages that had entered the germband and those with above 50% retraction  
1142 for the number along the ventral nerve cord (vnc), anterior tip of the head and in the  
1143 whole embryo. Macrophages were visualized using confocal microscopy with a Z-

1144 resolution of 3  $\mu\text{m}$  and the number of macrophages within the germband or the  
1145 segments of vnc was calculated in individual slices (and then aggregated) using the  
1146 Cell Counter plugin in FIJI. Total macrophage numbers were obtained using Imaris  
1147 (Bitplane) by detecting all the macrophage nuclei as spots.

#### 1148 **Image Processing and Analysis of macrophage migration**

1149 Embryos in which the macrophage nuclei were labeled with *srpHemo-*  
1150 *H2A::3XmCherry* were imaged and  $250 \times 130 \times 36 \mu\text{m}^3$  3D-stacks were typically  
1151 acquired with a constant  $0.5 \times 0.5 \times 1 \mu\text{m}^3$  voxel size at every 40-41 seconds for  
1152 approximately 3 hours. Images acquired from multiphoton microscopy were initially  
1153 processed with InInspector software (LaVision Bio Tec) to compile channels from the  
1154 imaging data, and the exported files were further processed using Imaris software  
1155 (Bitplane) to visualize the recorded channels in 3D. Briefly,

1156 i. The movie from each imaged embryo was rotated and aligned along the AP axis for  
1157 tracking analysis.

1158 ii. To calculate migration parameters while macrophages migrate from the head  
1159 mesoderm to the edge of the germband, movies were cropped in time to that period  
1160 (typically 60 minutes from the original movie was used for analysis).

1161 iii. Macrophage nuclei were extracted using the spot detection function and tracks  
1162 generated in 3D over time. We could not detect all the macrophages in the head  
1163 mesoderm as spots because of limitations in imaging parameters. Tracks of  
1164 macrophages which migrate towards the dorsal vessel, ventral nerve cord and to the  
1165 anterior of the head were omitted. The edge of the germband was detected using  
1166 autofluorescence from the yolk and the mean position of the tracks in X- and Y-axis  
1167 was used to restrict analysis to before macrophages reach the edge of the germband.

1168 iv. Nuclei positions in XYZ-dimensions were determined for each time point and used  
1169 for further quantitative analysis.

1170 v. To calculate the speed of migration of the first macrophage in the germband the  
1171 track generated for the first macrophage alone was utilized to obtain the nuclei  
1172 position in XYZ-dimensions. Speed calculated within the first 35-45  $\mu\text{m}$  of the  
1173 germband is shown in Figure 2M and within the next 35-45  $\mu\text{m}$  is shown in Figure  
1174 2N.

1175 Cell speeds and persistence was calculated in Matlab (The MathWorks Inc.) from  
1176 single cell positions in 3D for each time frame measured in Imaris (Bitplane), as  
1177 described elsewhere (Smutny et al., 2017). Briefly, instantaneous velocities from  
1178 single cell trajectories were averaged to obtain a mean instantaneous velocity value  
1179 over the course of measurement. To calculate persistence values, single cell  
1180 trajectories were split into segments of equal length ( $l$ ;  $l = 10$  frames) and calculated  
1181 via a sliding window as the ratio of the distance between the macrophage start-to-end  
1182 distance ( $D$ ) over the entire summed distance covered by the macrophage between  
1183 each successive frame ( $d_i$ ) in a segment. Calculated persistence values were averaged  
1184 over all segments in a single trajectory and all trajectories were averaged to obtain a  
1185 persistence index ( $I$ ) for the duration of measurement (with 0 being the lowest and 1  
1186 the maximum directionality) as follows:

$$I(l) = \sum_{k=1}^{n-l} \left( \frac{D_k / \sum_{i=k}^{k+l} d_i}{n-l} \right)$$

1187 where  $n$  represents the total number of frames,  $i$  the sum of frame-to-frame distances  
1188 over one segment and  $k$  the sum over all segments of a trajectory.

1189 Embryos expressing *srpHemo-3XmCherry* and *knock-in DE-Cadherin::GFP* were  
1190 used for calculating time for macrophage entry. Briefly,  $100 \times 130 \times 34 \mu\text{m}^3$  3D-stacks

1191 were typically acquired with a constant  $0.28 \times 0.28 \times 2 \mu\text{m}^3$  voxel size at every 40-41  
1192 seconds for approximately 3 hours. The time point when the macrophage protrusion  
1193 touched the edge of the germband was defined as T0 and the time point when the  
1194 entirety of the macrophage was within the germband was taken as T1 and T1-T0 was  
1195 defined as time for macrophage entry. T0 and T1 were determined by precisely  
1196 examining macrophage position in xy and z dimensions (examination of individual 2  
1197 micron slices) over time.

#### 1198 **Measurement of junctional fluorescence intensities**

1199 The apical junction intensity of Patj and Phospho-Myosin Regulatory Light Chain  
1200 were calculated using linescan analysis as previously described (Smutny et al., 2010)  
1201 with the following changes. The line length was approximately the cell length and the  
1202 line was always drawn from the outside of the cell to the inside. For every line, a  
1203 Gaussian fit was applied and intensities across the cell junction were then normalized  
1204 against the cytosolic signal using the PeakfitProfiles plugin in Fiji. Calculation of  
1205 mean intensity within the ectoderm-mesoderm interface for DE-Cadherin, N-  
1206 Cadherin, Laminin A, Dystroglycan,  $\beta$  PS integrin and Talin, and calculation of mean  
1207 intensity at the cell boundaries for Eiger was conducted as follows. Mean intensity  
1208 within a line (typically of line width 10 pixels) drawn at the interface or at the cell  
1209 boundary (for Eiger) was obtained in FIJI and then normalized to the cytosolic signal.  
1210 The levels of Eiger in the AS was quantified at all sagittal planes including those in  
1211 which the amnioserosa extends more broadly across the embryo in the anterior  
1212 posterior direction, thus more extensively covering the germband ectoderm. For both  
1213 junctional and interface analysis typically 30-40 interfaces / boundaries from 3-7  
1214 embryos were used for the analysis.

1215

## 1216 Tension measurements of cell junctions by UV laser ablation

1217 The apical tension of cell-cell contacts was assessed by conducting laser ablation on a  
1218 previously described Axio Observer Z1 (Zeiss) inverted microscope with a confocal  
1219 spinning disc unit for high speed imaging (Smutny et al., 2015) and a Plan Apo 63x  
1220 1.2 NA water-immersion lens (Zeiss). A pulsed 355 nm laser was used to ablate  
1221 apical cell junctions labeled with *knock-in DE-cadherin::GFP* in control, *egr<sup>1</sup>* and  
1222 *grnd<sup>Minos</sup>* mutant embryos when the macrophages were near the edge of the germband  
1223 but not within. UV ablations were operated by a custom-designed LabView software  
1224 to allow simultaneous control of image acquisition and laser ablation. A typical  
1225 ablation experiment was performed point-wise along a 6  $\mu\text{m}$  length line perpendicular  
1226 to and centered on an apical junction, using a laser pulse rate of 1kHz, an area density  
1227 along the line of 1 shot/ $\mu\text{m}^2$ , 25 pulses per ablation point with an average power of  
1228 15 $\mu\text{watt}$  and a total ablation duration between  $\sim$ 150-350 ms. Fluorescent images were  
1229 acquired for one channel (488 nm wavelength) with an iXon DU-897-BV camera  
1230 (Andor Technology) using exposure times and frame rates of 200ms. Laser ablation  
1231 itself lasted for  $\sim$ 250 ms and resulted in a local depletion of DE-Cadherin at the apical  
1232 cell cortex. Care was taken to ablate contacts without causing any damage to the  
1233 embryo, which was confirmed by monitoring embryos over an extended time period  
1234 without obvious detection of leakage of fluorescent cytoplasmic material, or cell  
1235 rupture and apoptosis. To inhibit Myosin activity, 100mM Rho-kinase inhibitor (Y-  
1236 27632 dihydrochloride, Tocris Bioscience) resuspended in water was injected  
1237 laterally into the perivitelline space of Stage 11 embryos after germband extension  
1238 was complete. To assess the recoil of apical DE-Cadherin in response to laser  
1239 ablation, we first post-processed all raw images from laser ablation with Fiji software  
1240 by subtracting measured mean background values and applied a Gaussian filter before



1241 using a kymograph analysis of a segmented line defining DE-Cadherin along the  
1242 ablated apical cell cortex. The minimum intensity of apical DE-Cadherin was  
1243 measured pre-cut to threshold the kymograph for post-cut analysis. The two open end  
1244 tips of apical cortical DE-Cadherin after ablation were tracked for the first frame after  
1245 opening ( $t_0$ ) and every consecutive 0.8 seconds ( $t_n$ ) to calculate the total distance  $d$   
1246 ( $\mu\text{m}$ ) of the opening for every time point. The recoil distance ( $R$ ) of each end tip at a  
1247 given time point ( $t_n$ ) was calculated as follows:

$$\frac{d(t_n) - d(t_0)}{2} = R(t_n)$$

1248 The initial recoil velocity  $RV$  ( $\mu\text{m/s}$ ) for each cut was derived by calculating the  
1249 recoil distance for the primary opening frame ( $t_1$ ) post-cut as follows:

$$\frac{d(t_1) - d(t_0)}{2 t_1} = RV$$

1250 Measurements were processed in Prism (Graphpad) and Matlab (R2013a; Mathworks)  
1251 for calculations and plotting of graphs. For curve fitting of recoil distances, we used  
1252 nonparametric fitting with a smoothing spline model through the calculated data.

### 1253 **CellFIT-3D interfacial tension analysis**

1254 CellFIT provides a general-purpose mathematical formalism for calculating the forces  
1255 that produce specific observed cell and tissue motions and geometries, which was  
1256 recently adapted to a 3D system (Brodland et al., 2014; Krens et al., 2017). For the  
1257 CellFIT-3D analysis, we acquired confocal image stacks of fixed Stage 11 embryos  
1258 that were oversampled in the z-direction ( $0.5 \mu\text{m}$  steps), to increase the number of  
1259 triple cell junctions that could be annotated per cell. In short, to obtain estimates of  
1260 the relative edge tensions, the angles at triple junctions, such as those between apical,  
1261 basal and the lateral interfaces of the germ band ectoderm cells, were manually  
1262 digitized using custom software. The angles along particular cells edges were

1263 digitized in multiple images within the stack in order to obtain the true angles of the  
1264 cell membranes with the edge (see Movie S6). We analysed 70 control (n=5 embryos)  
1265 and 79 *egr*<sup>1</sup> (n=4 embryos) triple cell junctions, an that, in average, consists of ~5  
1266 annotated triplets (Z-planes) per analysed triple cell junction annotation, resulting in a  
1267 total of approximately 750 cell manually annotated triplets. Force-balance equations  
1268 were written for each digitized triple junction as described previously (Krens et al.,  
1269 2017), and least-squares solutions were found for all such equations. The solutions to  
1270 these equations provided the relative strengths of the tensions along each edge type  
1271 (Krens et al., 2017). The averaged values provided were used as the relative strengths  
1272 of the tensions along each edge type.

### 1273 **Cell segmentation and deformation analysis**

1274 Embryos expressing *srpHemo-3XmCherry* and *knock-in DE-Cadherin::GFP* were  
1275 used for cell segmentation. Briefly, 100x130x34 $\mu\text{m}^3$  3D-stacks were typically  
1276 acquired with a constant 0.28x0.28x1.5 $\mu\text{m}^3$  voxel size at every 40-41 seconds for  
1277 approximately 3 hours. Fragments of multiphoton movies showing the initial stages of  
1278 macrophage penetration through the ectoderm were selected. To facilitate 2D  
1279 segmentation of ectoderm cell bodies, we used the Ilastik 1.1.8 program. Pixel  
1280 classification project was trained to distinguish between cell bodies and cell  
1281 membrane, using full range of neighborhood analysis parameters presented in Ilastik  
1282 1.1.8, with a deviation  $\sigma=3$ . After training on 15 reproducible images of the ectoderm,  
1283 the remaining ectoderm images were batch-processed and images containing the  
1284 probabilities of pixels belonging to the ‘membrane’ or the ‘cytosol’ area were  
1285 exported and used for intensity-based segmentation. In some areas, the segmentation  
1286 had to be corrected manually in the final binary images. Ectoderm membranes that

1287 appeared inside of the macrophages were manually removed from the segmented  
1288 image to avoid including apoptotic cells in the final analysis.  
1289 The resulting binary images were analyzed using a custom Matlab R2015b script;  
1290 they were preprocessed using a set of bwmorph functions to remove spurious pixels  
1291 and single-pixel bridges between the separate cells. Then the length-to width ratio of  
1292 an ellipse encircling each ectodermal cell was calculated using ectodermal cells that  
1293 were not adjacent to the image border. The length-to-width ratio was defined as a  
1294 ratio of regionprops.MajorAxisLength to regionprops.MinorAxisLength for each cell  
1295 (Figure S6F). To understand how deformation in the neighborhood of a macrophage  
1296 occurs, we analyzed the length-to-width ratio of ectoderm cells with centroids located  
1297 not further than 10 $\mu$ m from the nearest edge of a macrophage (Figure 6H). The  
1298 significance of the length to width ratio distribution differences between cells in the  
1299 control and the *egr<sup>1</sup>* mutant (Figure 6H) was analyzed with an unpaired t-test  
1300 assuming normal distribution.

## 1301 **QUANTIFICATION AND STATISTICAL ANALYSIS**

### 1302 **Statistical Analysis**

1303 Statistical tests as well as the number of embryos/ cells assessed are listed in the  
1304 Figure legends. All statistical analyses were performed using GraphPad Prism and  
1305 significance was determined using a 99% confidence interval. No statistical method  
1306 was used to predetermine sample size and the experiments were not randomized.  
1307 Data points from individual experiments / embryos were pooled to estimate mean and  
1308 s.e.m. Error bars in all graphs represent the standard error of the mean. An unpaired t-  
1309 test was used to calculate the significance in differences between two groups and  
1310 One-Way ANOVA followed by Dunnett or Tukey post tests were used for multiple  
1311 comparisons.

1312 **Repeatability**

1313 All measurements were performed in 3-40 embryos. Representative images shown in  
1314 Figure 1D,E,I,J Figure 2B, Figure 3A,A'B,B',F,G, Figure 4B,E,F,G, Figure 5B,D,J,  
1315 Figure S2A,D,E,F, Figure S3A,A'B,B',H, Figure S4C,E,I,J,K, Figure S5A,B,D,E and  
1316 Figure S6E were from experiments that were repeated at least 3 and up to 7 times.  
1317 Representative *in situ* images shown in Figure 2A were from an experiment repeated  
1318 3 times and those in Figure 3E were from an experiment repeated 2 times.  
1319 Representative TEM images shown in Figure 1E,H and Figure S1D,E were from an  
1320 experiment repeated 3 times. Representative images showing macrophage migration  
1321 tracks color coded for persistence in Figure S2M,O and 3E and stills shown in Figure  
1322 1C, Figure 2J, Figure 3H, and Figure S6F are from two-photon movies, which were  
1323 repeated at least 3 times. Representative Images shown in Figure 6B,C and Figure  
1324 S6A are stills from confocal spinning disc movies which were repeated at least 8  
1325 times.

1326

1327

1328 **Movies**

1329 **Movie S1: Macrophages invade into the germband by transiently separating**  
1330 **apposing tissues, related to Figure 1C.**

1331 Two-photon time-lapse imaging *e22c-GAL4 srpHemo-3xmCherry; 10xUAS-*  
1332 *CD8::GFP* embryos where CD8-GFP labels membranes (green) and 3XmCherry  
1333 labels macrophages (red). The embryo is oriented with anterior to the left and dorsal  
1334 up and the area imaged in the embryo is indicated in the grey box in the schematic  
1335 Figure 2D. The time interval between each acquisition is 40 seconds and the display  
1336 rate is 10 frames per second. Scale bar represents 25µm.

1337

1338 **Movie S2: Macrophage migration into the germband in control (con), *egr<sup>1</sup>* and**  
1339 *grnd<sup>Minos</sup>* embryos, related to Figure 2J and 3H.

1340 Representative two-photon movies of control (con) embryos (*srpHemo-*  
1341 *H2A::3xmCherry*), *egr<sup>1</sup>* (*egr<sup>1</sup>; srpHemo-H2A::3xmCherry*) and *grnd<sup>Minos</sup>* (*grnd<sup>Minos</sup>;*  
1342 *srpHemo-H2A::3xmCherry*) embryos showing macrophage nuclei (red) migrating  
1343 from the head into the germband. The migration was imaged for 2 hours and the  
1344 embryo is oriented with anterior to the left and dorsal up. The area imaged in the  
1345 embryo is indicated in the schematic in Figure 1J. The line indicates the position of  
1346 the germband at selected time points. The time interval between each acquisition is 40  
1347 seconds and the display rate is 20 frames per second. Scale bar represents 25µm.

1348

1349 **Movie S3: Tracking macrophage migration from head to the germband in**  
1350 **control (con), *egr<sup>1</sup>* and *grnd<sup>Minos</sup>* embryos, related to Figure 2G-I, Figure S2 L,M and**  
1351 **Figure S3D-G.**

1352 Representative movies of control (con) embryos (*srpHemo-H2A::3xmCherry*), *egr<sup>1</sup>*  
1353 (*egr<sup>1</sup>; srpHemo-H2A::3xmCherry*) and *grnd<sup>Minos</sup>* (*grnd<sup>Minos</sup>; srpHemo-*  
1354 *H2A::3xmCherry*) embryos showing macrophage nuclei (red) migrating from the  
1355 head up to the edge of the germband. Superimposed are the macrophage nuclei  
1356 detected as spots (grey) and dragon tail tracks showing the migration of the  
1357 macrophages over time. Each dragon tail shows macrophage migration behavior for 5  
1358 time points. The time interval between each acquisition is 40 seconds and the display  
1359 rate is 10 frames per second. Scale bar represents 10µm.

1360

1361 **Movie S4: Macrophage invasion into the germband is a time intensive process,**

1362 **related to Figure 2K.**

1363 Representative two-photon movie showing macrophage invasion into the germband in  
1364 control embryos (*DE-Cadherin::GFP; srpHemo-3xmCherry*). A z-projection of 7 slices  
1365 (2µm each) is shown. The time point when the macrophage protrusion touched the  
1366 edge of the germband was defined as T0 (time point 50, arrow) and the time point  
1367 when the entirety of the macrophage was within the germband (determined by the  
1368 examination of the macrophage in individual slice and time) was taken as T1 (time  
1369 point 90, arrowhead). T1-T0 was defined as the time for macrophage entry. T0 and T1  
1370 were determined by precisely examining macrophage position in xyz dimensions over  
1371 time. The time interval between each acquisition is 41 seconds and the display rate is  
1372 5 frames per second. Scale bar represents 25µm.

1373

1374 **Movie S5: Laser ablation of the germband ectoderm cells, related to Figure 6A-C**  
1375 **and Figure S6A.**

1376 Representative confocal spinning disc movies showing laser ablation of the  
1377 ectodermal apical DE-Cadherin::GFP in control, *egr<sup>1</sup>* and *grnd<sup>Minos</sup>* embryos, each  
1378 carrying *srpHemo-3xmCherry* to label macrophages and *knock-in DE-*  
1379 *Cadherin::GFP*. The time interval between each acquisition is 200 milliseconds and  
1380 the display rate is 5 frames per second. Scale bar represents 10µm.

1381

1382 **Movie S6: CellFIT-3D analysis, related to Figure 6.**

1383 Movie showing consecutive slices from confocal microscopy image of a fixed control  
1384 Stage 11 embryo with macrophage nuclei labeled by the expression of *srpHemo-*  
1385 *H2A::3XmCherry* and ectoderm cells visualized by immunolabeling for DE-Cadherin.  
1386 Representative cell triple interfacial junctions at apical and basal interfaces of a few

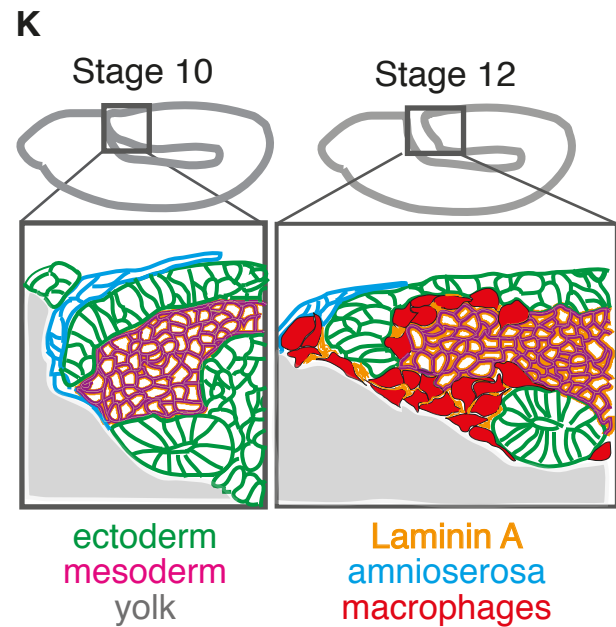
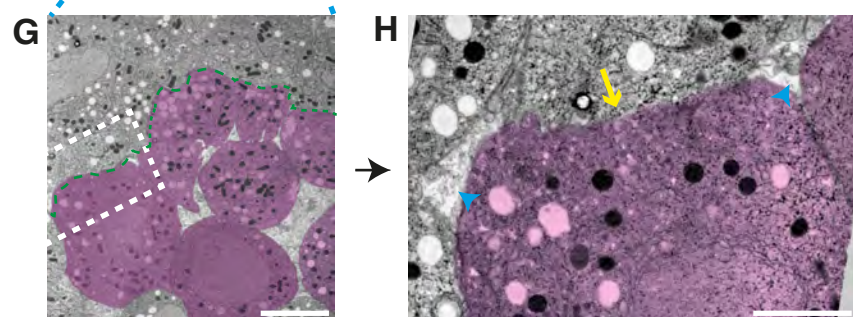
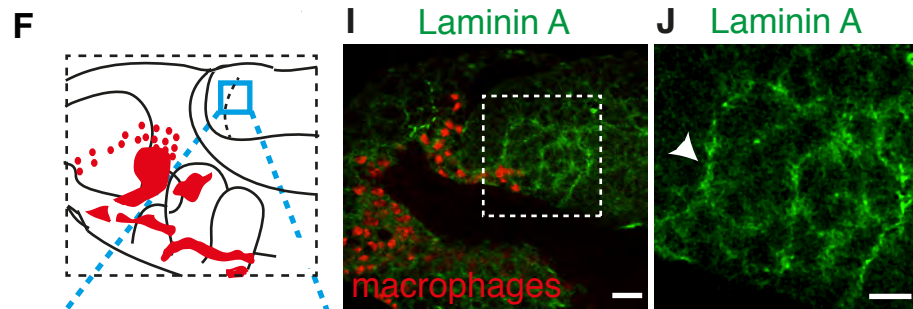
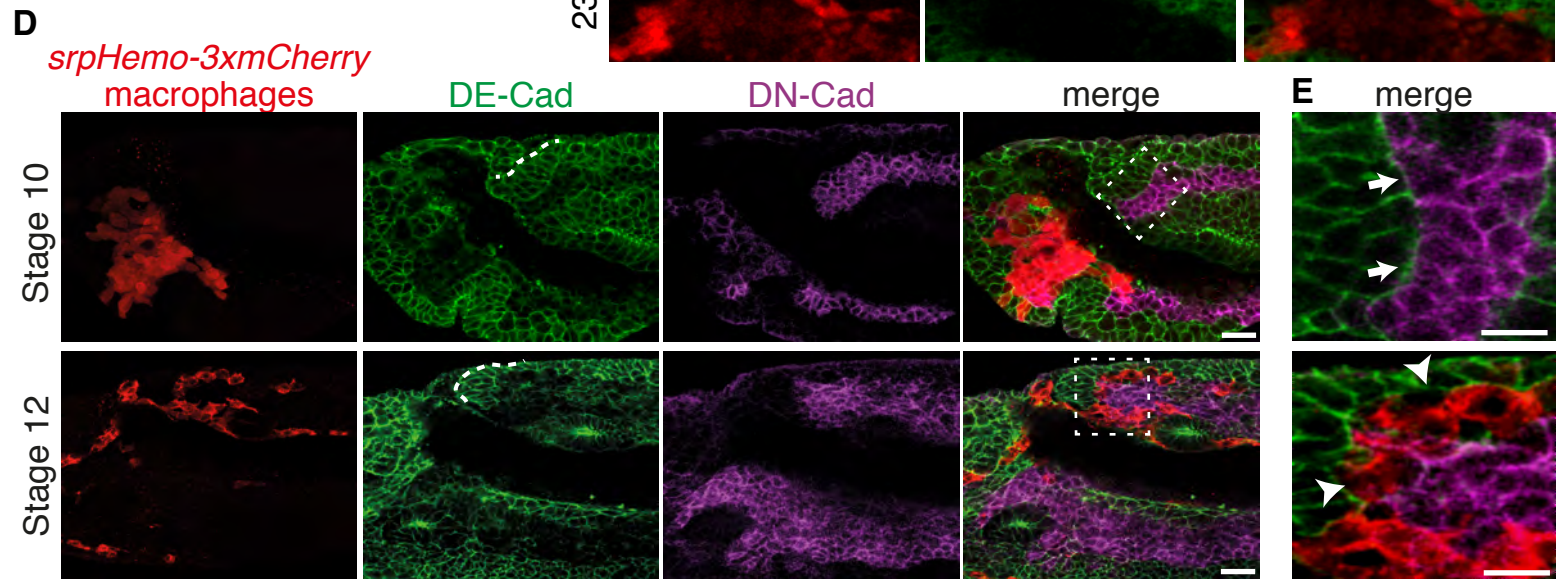
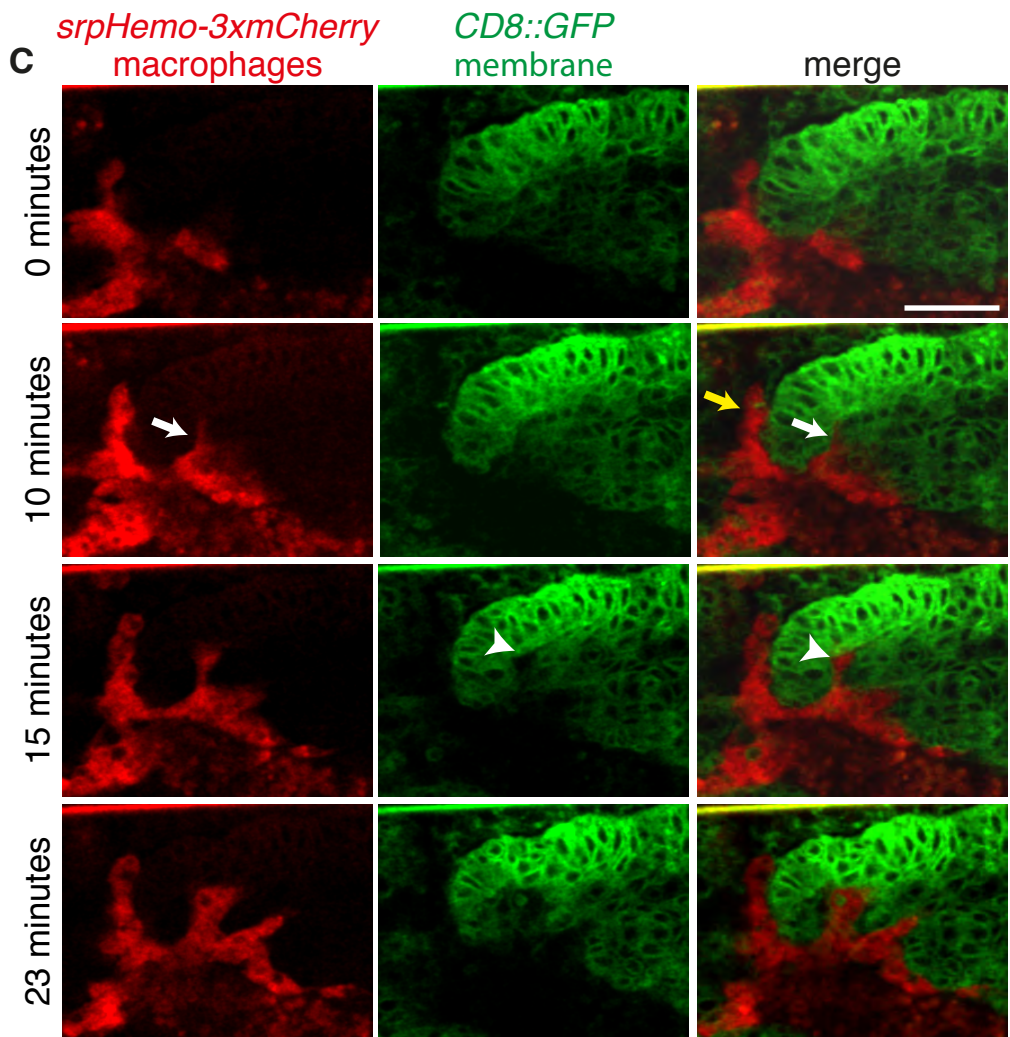
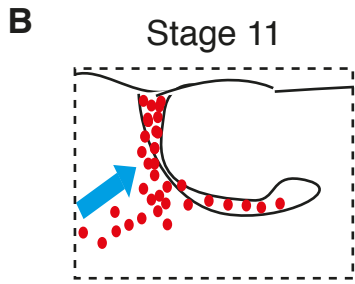
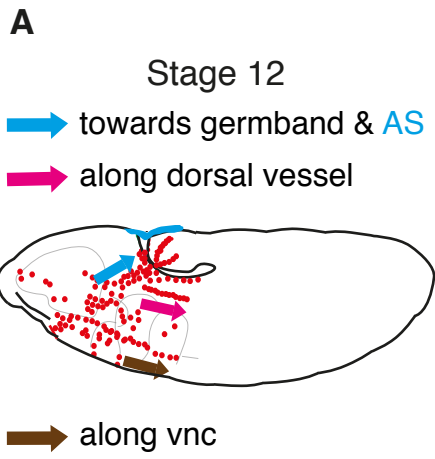
1387 cells in the germband ectoderm used for CellFIT-3D based tension analysis are  
1388 displayed. The display rate is 4 frames per second and the scale bar represents 10 $\mu$ m.

1389

1390 **Movie S7: Macrophages in *egr*<sup>1</sup> embryos are unable to effectively deform the**  
1391 **ectodermal cells during invasion into the germband, related to Figure 6H and**  
1392 **Figure S6F.**

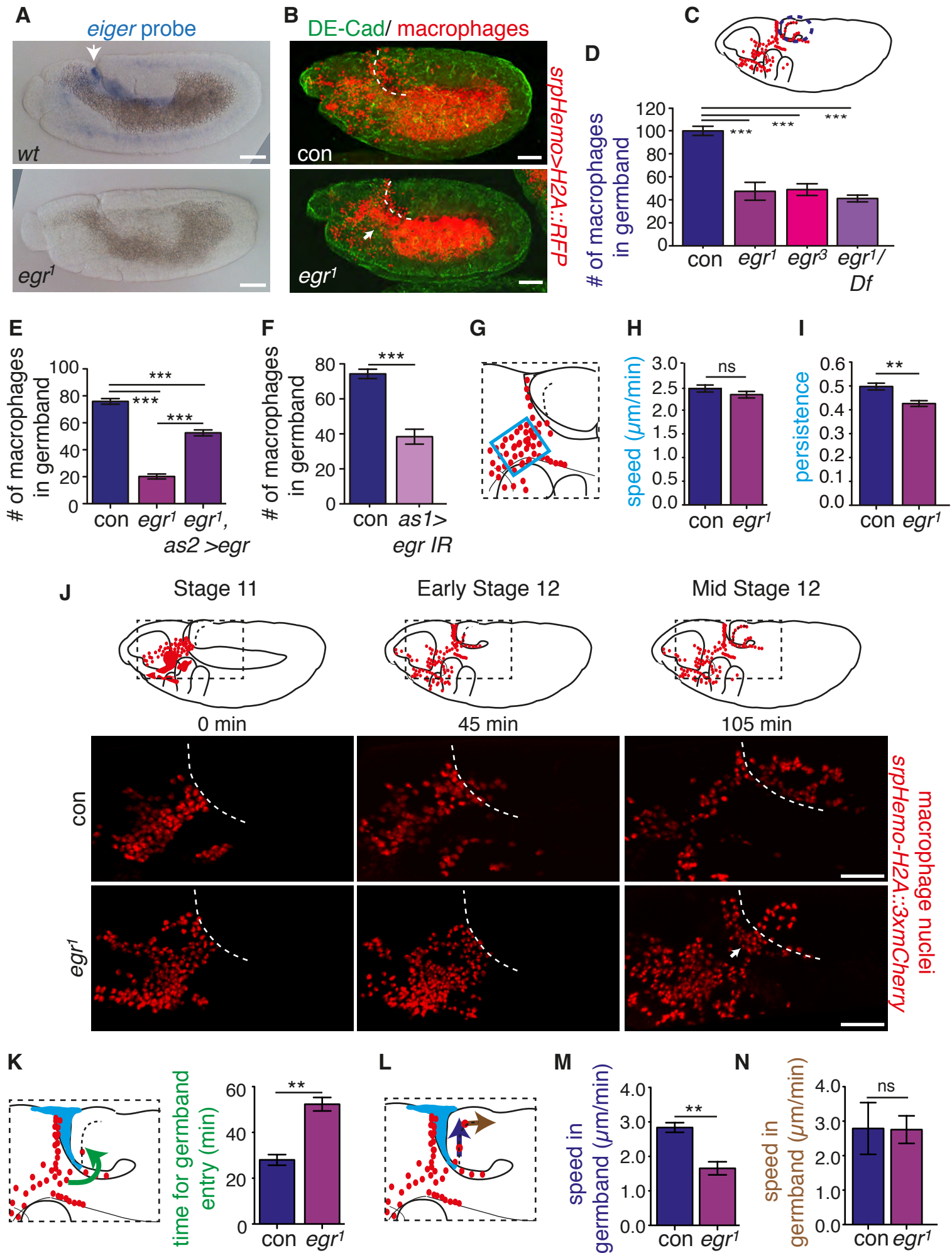
1393 Movie showing changes in the length/ width ratio (LWR) from before to after  
1394 macrophage invasion in control (con) and *egr*<sup>1</sup> embryos carrying *srpHemo-*  
1395 *3xmCherry* to label macrophages and the *knock-in DE-Cadherin::GFP* to visualize  
1396 cell edges. The macrophage (indicated by the white ROI) appears at time point 3. The  
1397 length/ width ratio (LWR) of the ectodermal cells is shown color-coded on a scale  
1398 from 1 to 4, with 1 representing a circular shape. The area imaged in the embryo is  
1399 indicated in the schematic in Figure 5G. The time interval between each acquisition is  
1400 40 seconds and the display rate is 5 frames per second. Scale bar represents 10 $\mu$ m.

# Siekhaus Figure 1

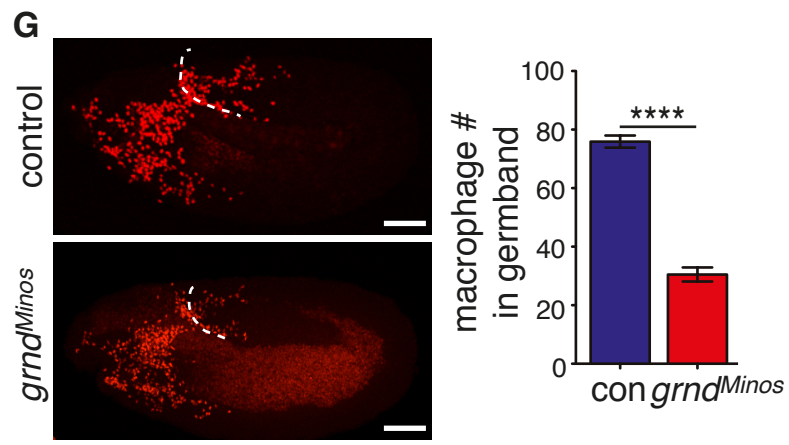
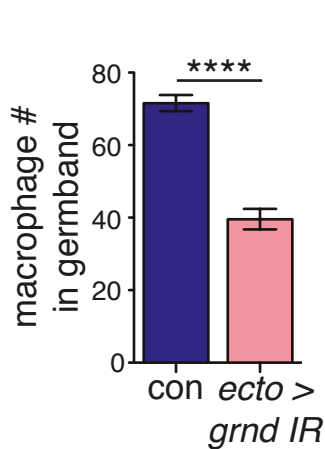
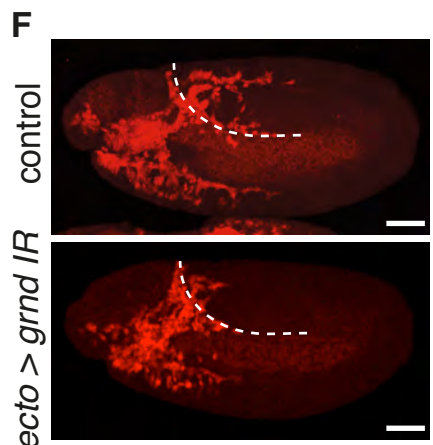
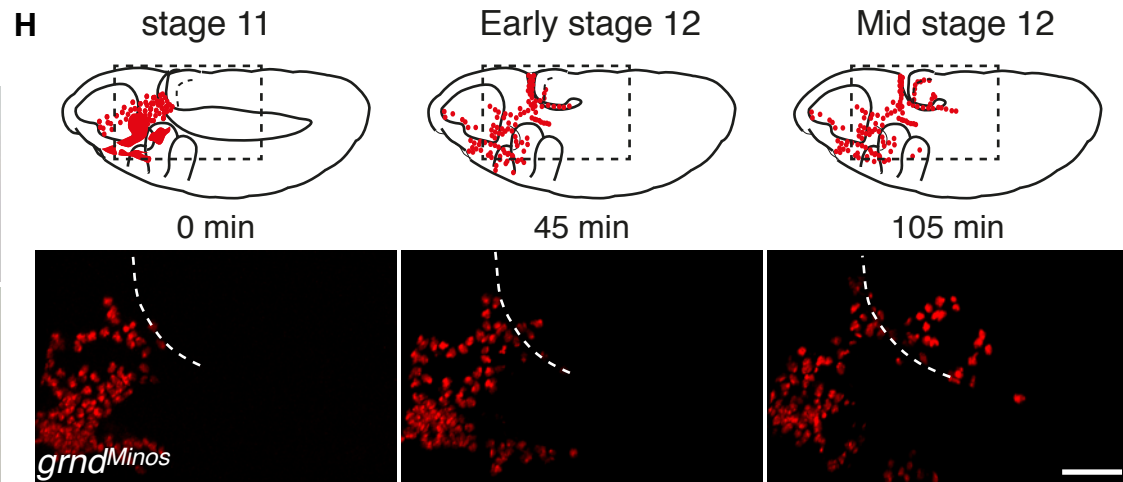
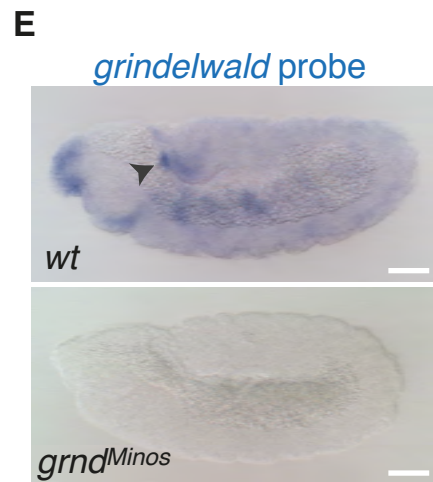
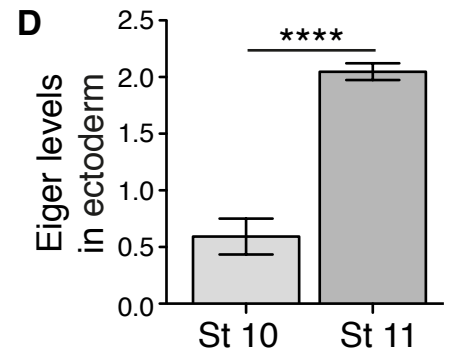
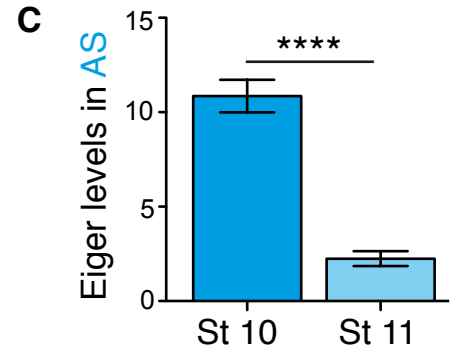
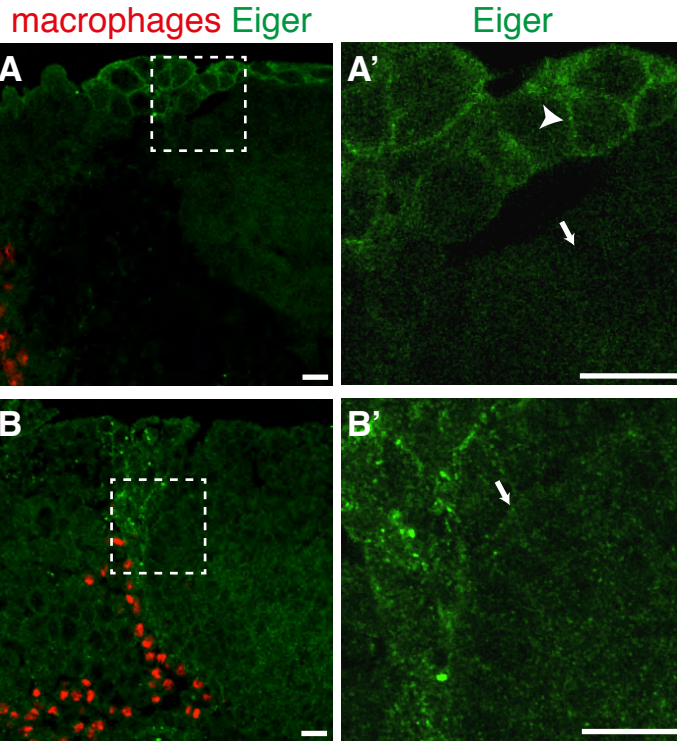




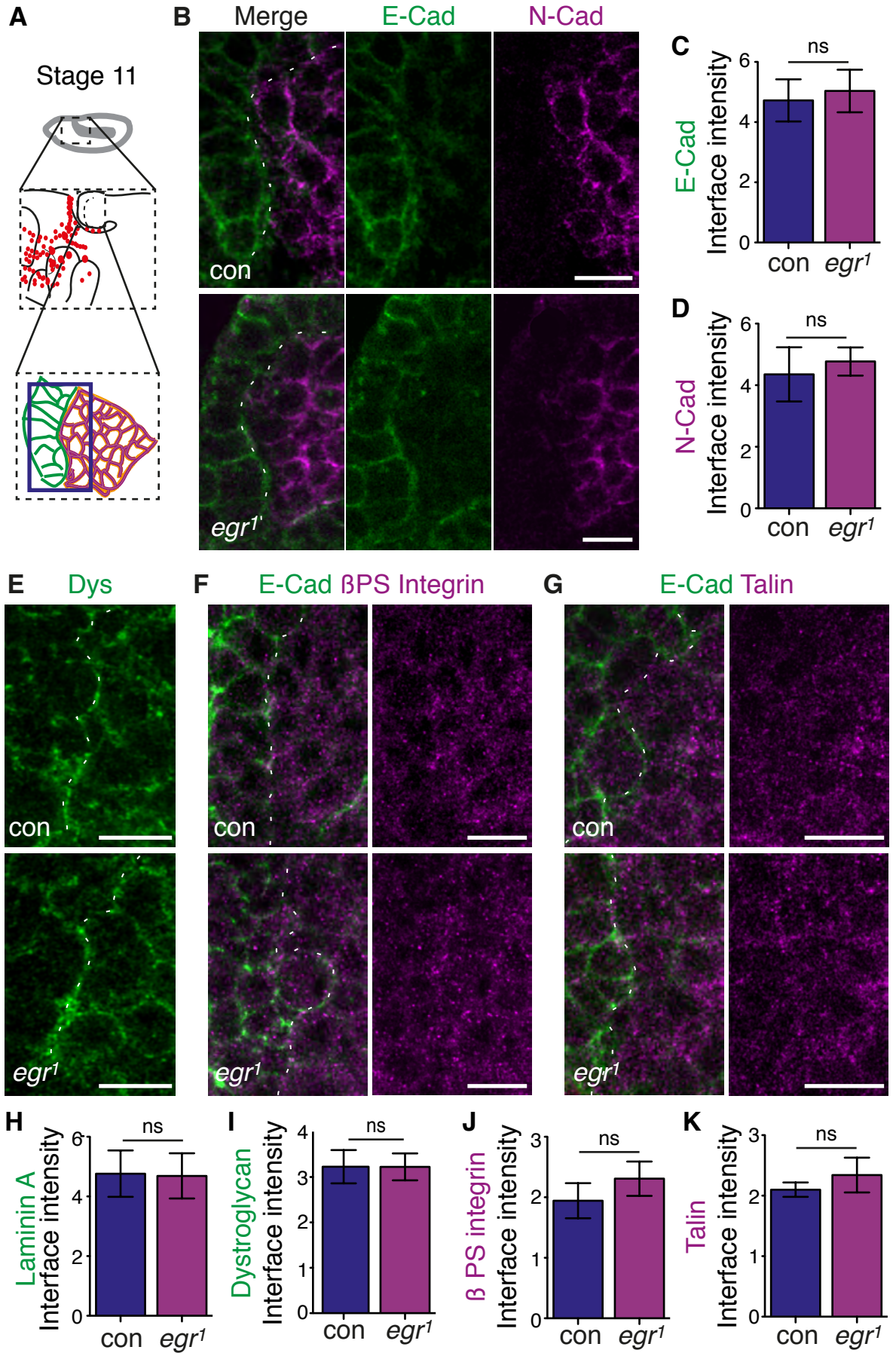
# Siekhaus Figure 2



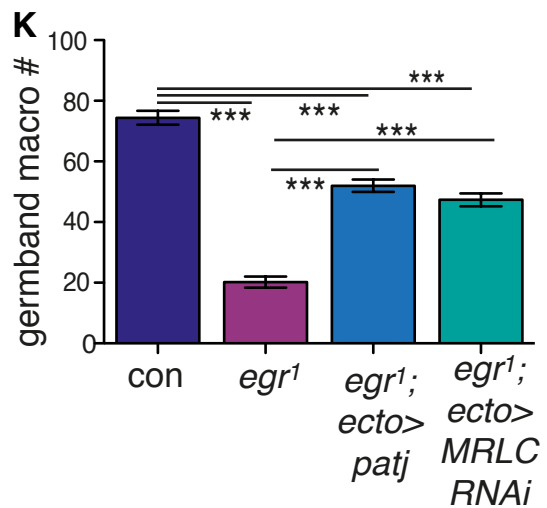
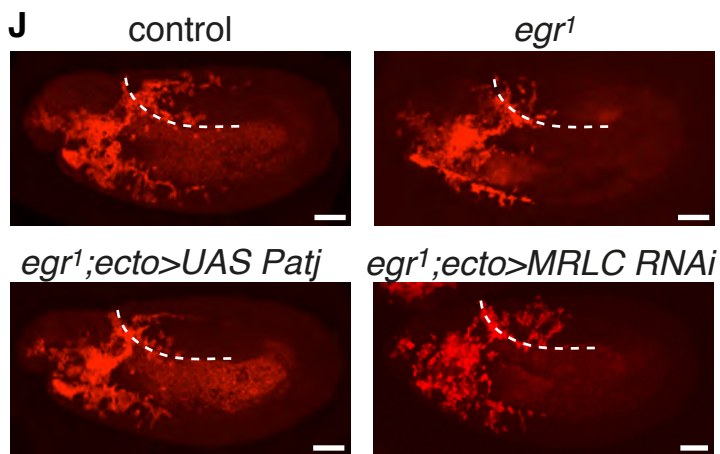
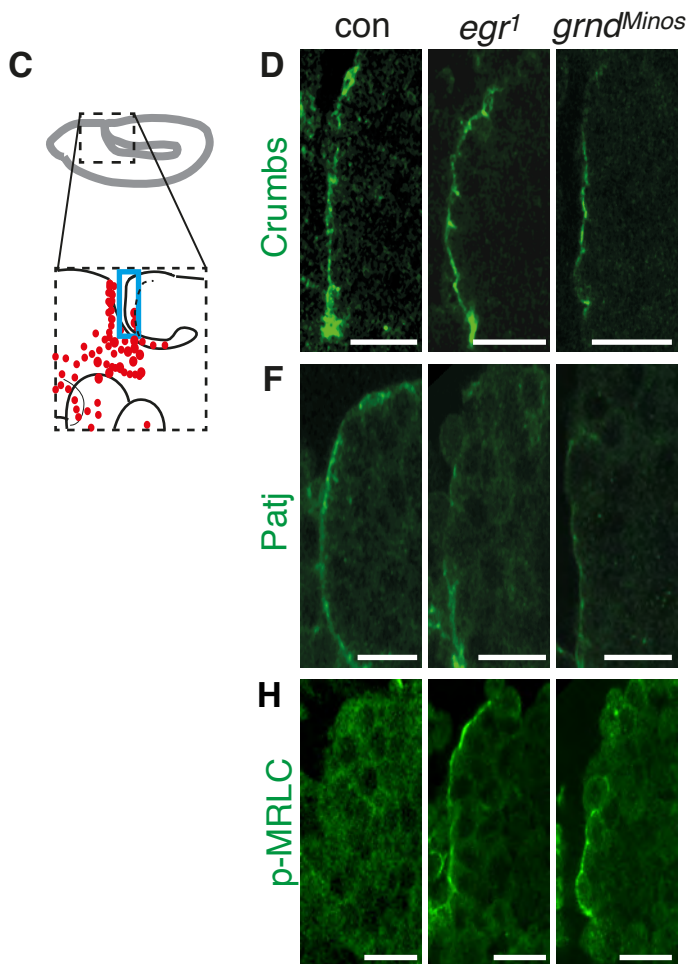
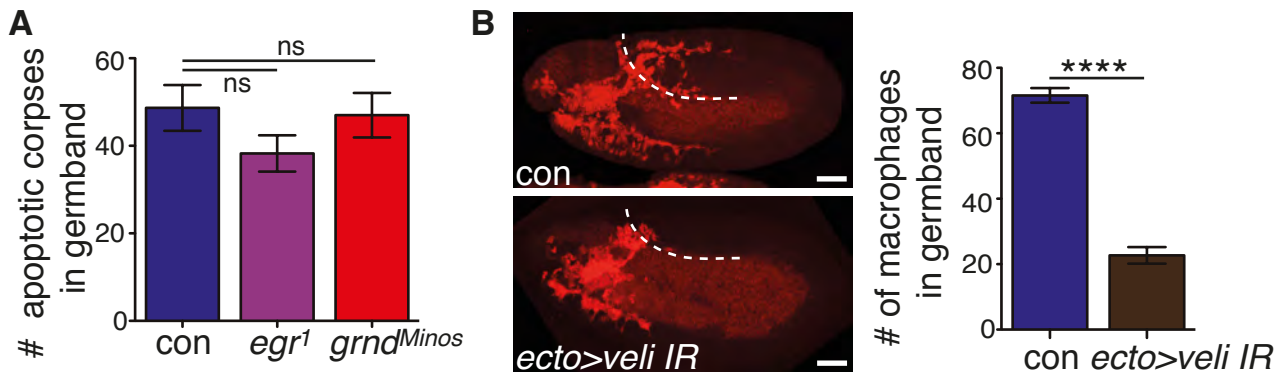
# Siekhaus Figure 3



# Siekhaus Figure 4



# Siekhaus Figure 5



# Siekhaus Figure 6

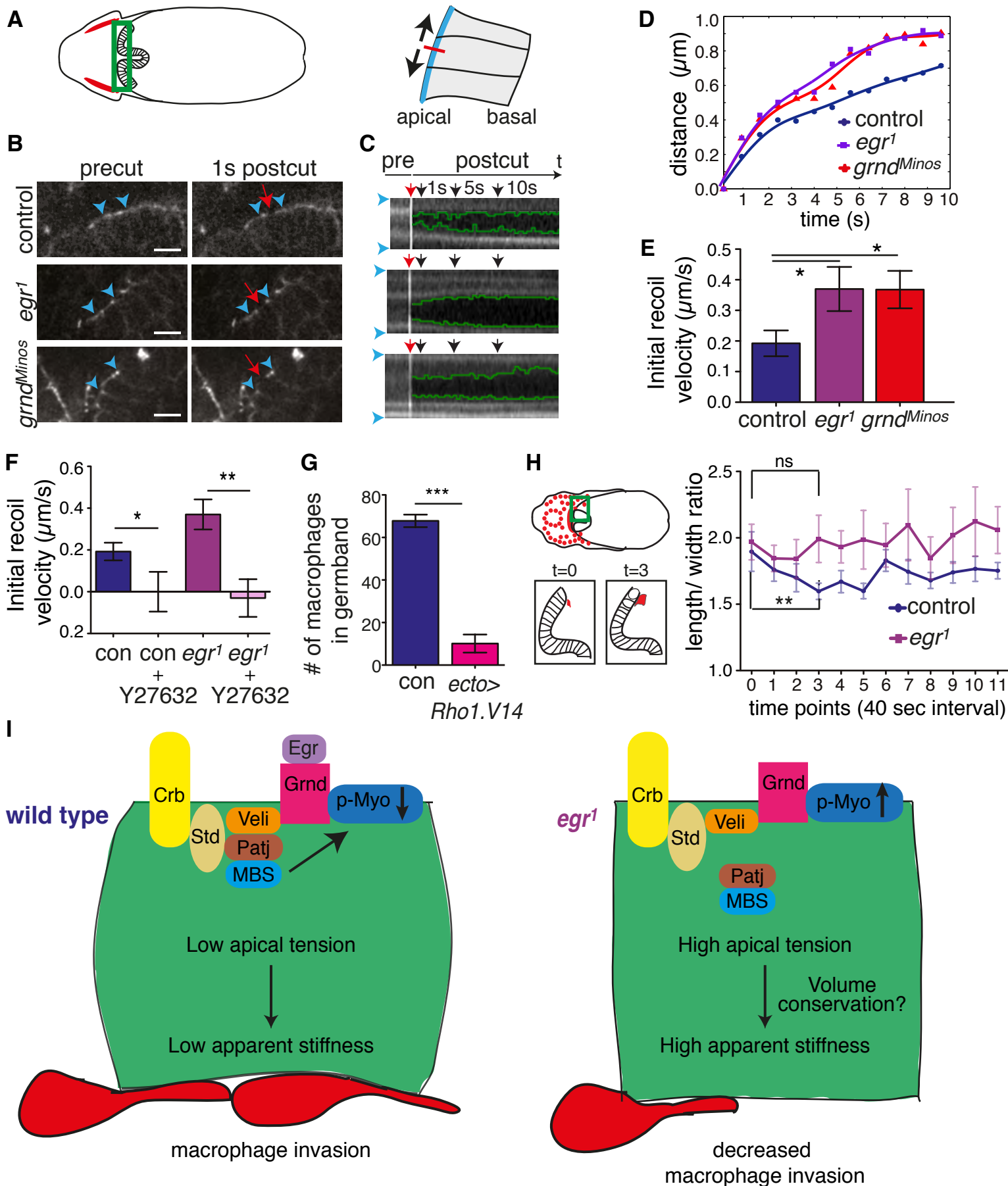
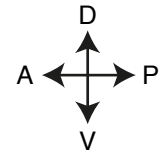
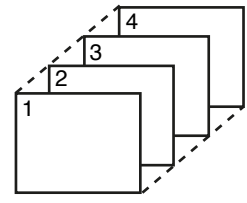
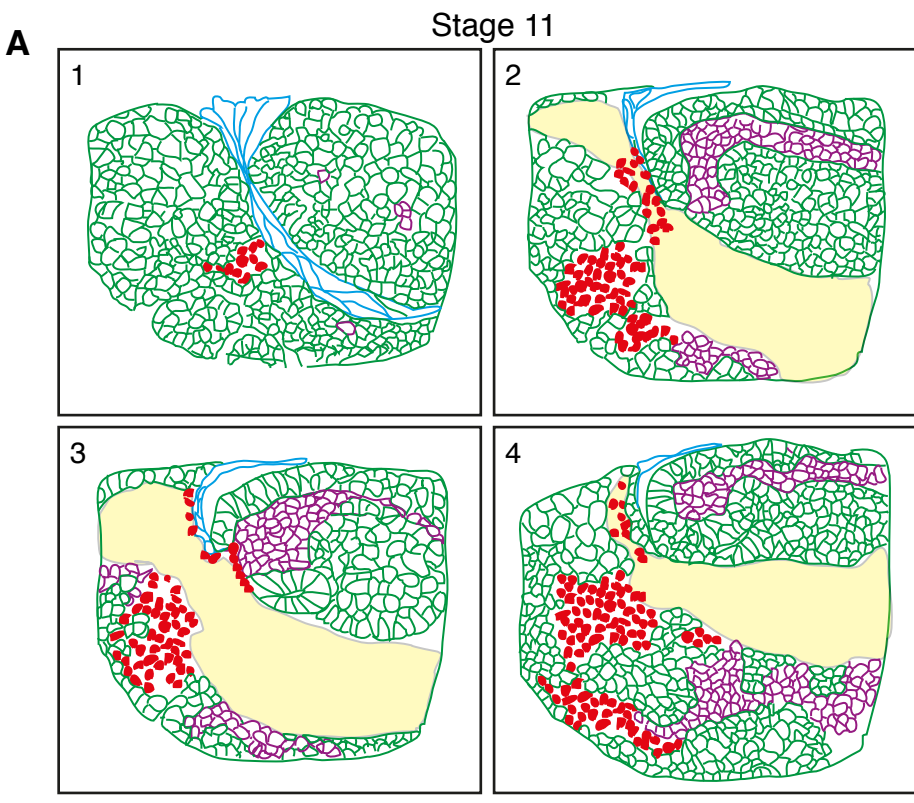
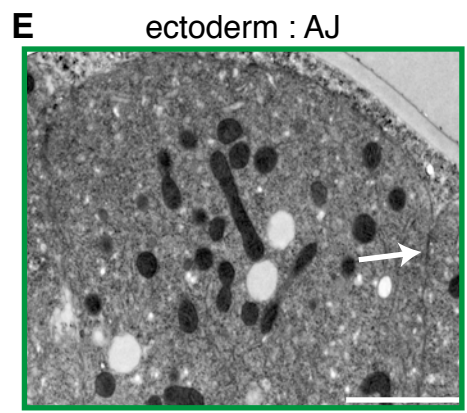
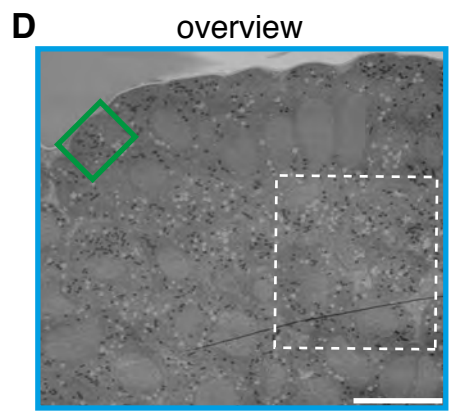
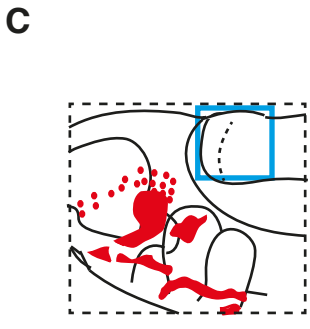
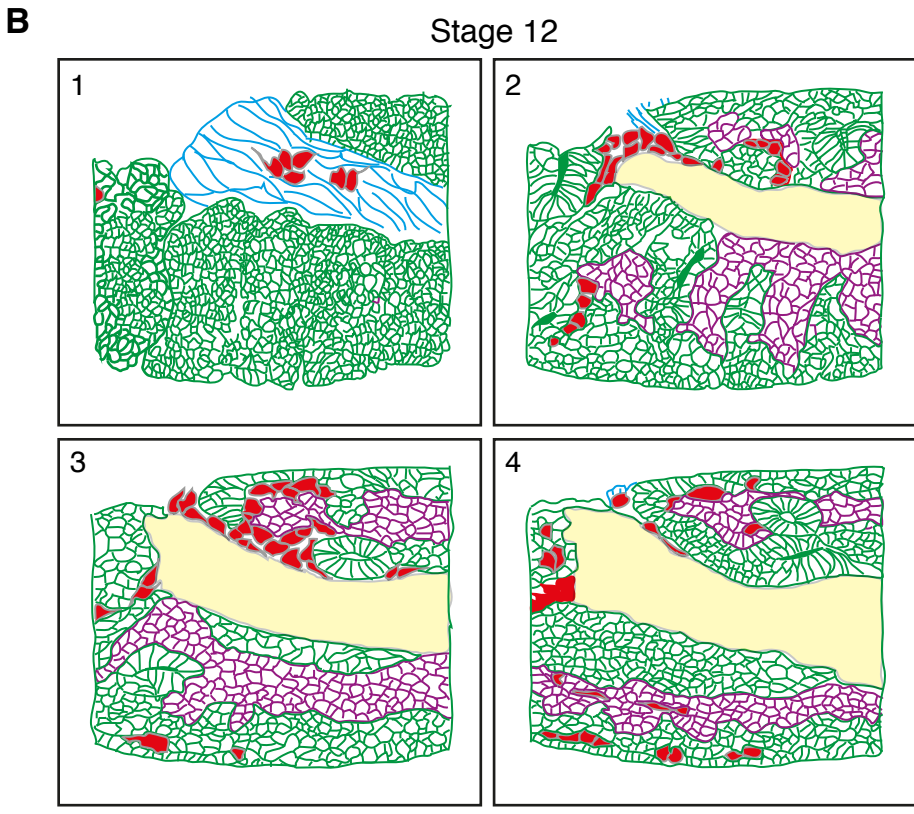


Figure S1



ectoderm  
mesoderm  
amnioserosa  
yolk  
macrophages



**Figure S1: Macrophages invade at the ectoderm-mesoderm interface in the germband. Related to Figure 1.**

**(A,B)** Cartoons showing consecutive sagittal sections (1-4) of a **(A)** Stage 11 or **(B)** Stage 12 *Drosophila* embryo. Embryo is shown with anterior to left and dorsal up. A: anterior, P: posterior, D: dorsal, V: ventral. Ectoderm (green), mesoderm (purple), yolk (yellow), amnioserosa (blue) and macrophages (red) are depicted.

**(C)** Schematic drawing of a lateral Stage 10 embryo with macrophages depicted as red dots. The black dotted line within the germband in the schematic indicates the ectoderm-mesoderm interface. Blue box indicates the area visualized in **(D)**, a Transmission electron microscopy (TEM) image of the germband of an early embryo in which the macrophages have not yet reached the germband. A magnification of the region indicated within the white dotted box is shown in Figure 1G. **(E)** TEM image showing a magnification of the area shown within the green box in **D**. White arrow indicates the presence of Adherens Junctions between ectodermal cells.

Embryo is shown with anterior to left and dorsal up. Embryos were selected for Stage 11 if they displayed germband retraction away from the anterior of 29-31% and for Stage 12 retraction of 35-40%. Scale bar represents 10 $\mu$ m in **D** and 2 $\mu$ m in **E**.

Figure S2

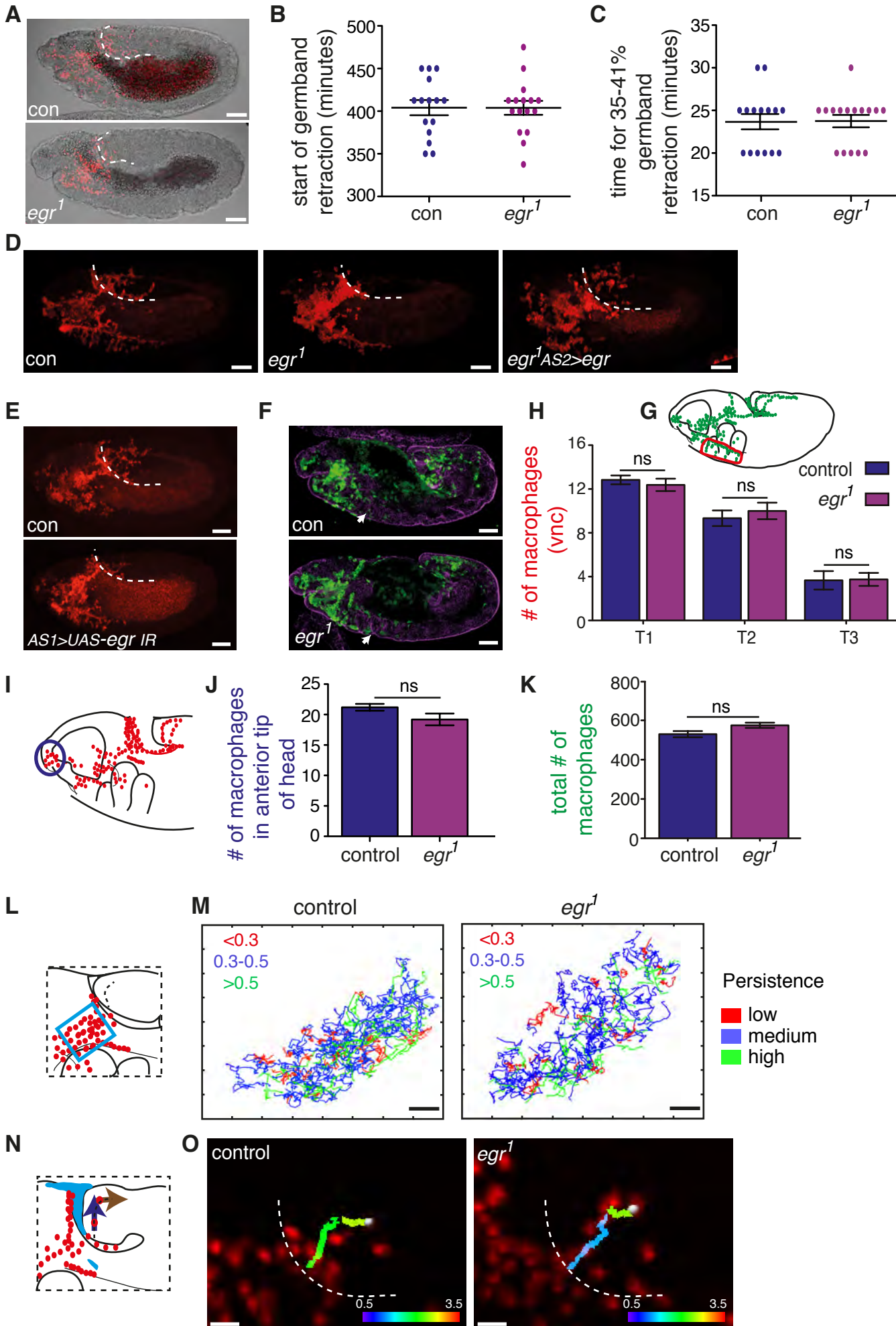




**Figure S2: Amnioserosal Eiger regulates macrophage invasion of the embryonic germband but not migration along the vnc. Related to Figure 2.**

(A) Confocal microscopy images of Z-projections of fixed lateral Stage 12 embryos. Control and *egr<sup>1</sup>* mutant embryos are shown, with macrophages labeled in red by the expression of *srpHemo>H2A::RFP* and the embryo visualized with transmitted light. The dotted line demarcates the edge of the germband.

(B,C) Quantifications showed no significant change in either the start of the initiation of germband retraction (B, minutes after egg laying) or the time taken to complete 35-41% of germband retraction (C, minutes). n=15 for control and 16 for *egr<sup>1</sup>* embryos.

(D,E) Confocal microscopy images of Z-projections of fixed lateral Stage 12 embryos. Macrophages are labeled in red by the expression of *srpHemo-H2A::3xmCherry*. The dotted line indicates the edge of the germband. AS stands for amnioserosa. (D) Control, *egr<sup>1</sup>* mutant, and *egr<sup>1</sup>* mutant embryos expressing *UAS-eiger* under the control of the LP1 amnioserosal driver, which was able to partially rescue the mutant phenotype. (E) Control embryos and those in which the amnioserosal *c381-Gal4* driver directs the expression of an RNAi against *eiger*.

(F) Confocal microscopy images of control and *egr<sup>1</sup>* fixed lateral late Stage 12 embryos with macrophages labeled in green by the expression of *srpHemo>GFP*. Arrows point to the macrophages migrating along the vnc. (G) Schematic drawing of a lateral late Stage 12 embryo depicting macrophages with green dots. The red dotted area indicates the area analyzed to count the number of macrophages in the ventral nerve cord (vnc). (H) Quantification reveals that the number of macrophages migrating along the vnc is not significantly affected by the *egr<sup>1</sup>* mutation. n=15 embryos for both genotypes.

(J) The number of macrophages in the anterior tip of the head (area within the blue circle in schematic I) and (K) the total number of macrophages within the entire embryo are not significantly affected by the *egr<sup>1</sup>* mutation. n=20 for all genotypes in J,K.

(L) Schematic of the anterior half of a lateral Stage 11 embryo indicating the region analyzed (area within blue box) to assess the persistence of macrophage migration up to the germband in the two-photon movie tracks shown in the right two panels. (M) Representative tracks of macrophages in control and *egr<sup>1</sup>* embryos from cell tracking in the region shown in blue box in L, color-coded according to low (<0.3; red), medium (0.3-0.5; blue) and high (>0.5; green) persistence of movement. n=3 embryos for both genotypes.

(N) Schematic indicating the regions of the germband in which the migration of the first macrophage was quantified. The amnioserosa (AS) is shown in light blue. The migration along the region adjacent to the amnioserosa is shown with a dark blue arrow and further migration along the germband with a brown arrow. (O) Tracks color-coded for mean instantaneous speed ( $\mu\text{m}/\text{min}$ ) during migration within the region of the germband adjacent to the AS and further migration along the germband in control and *egr<sup>1</sup>* embryos. n=3 embryos for both genotypes.

Anterior to left and dorsal up in all panels. The black dotted line within the germband in the schematics shown in G,I,L,N indicates the ectoderm-mesoderm interface. Embryos were selected for imaging and quantification as being Stage 11 if they displayed germband retraction away from the anterior of 29-31% and Stage 12 with 35-40%. Scale bar represents 50 $\mu\text{m}$  in A,D,E,F and 10 $\mu\text{m}$  in M,O. Histograms show mean  $\pm$  s.e.m. ns=not significant. Unpaired t-test for B,C,H,J,K.

Figure S3

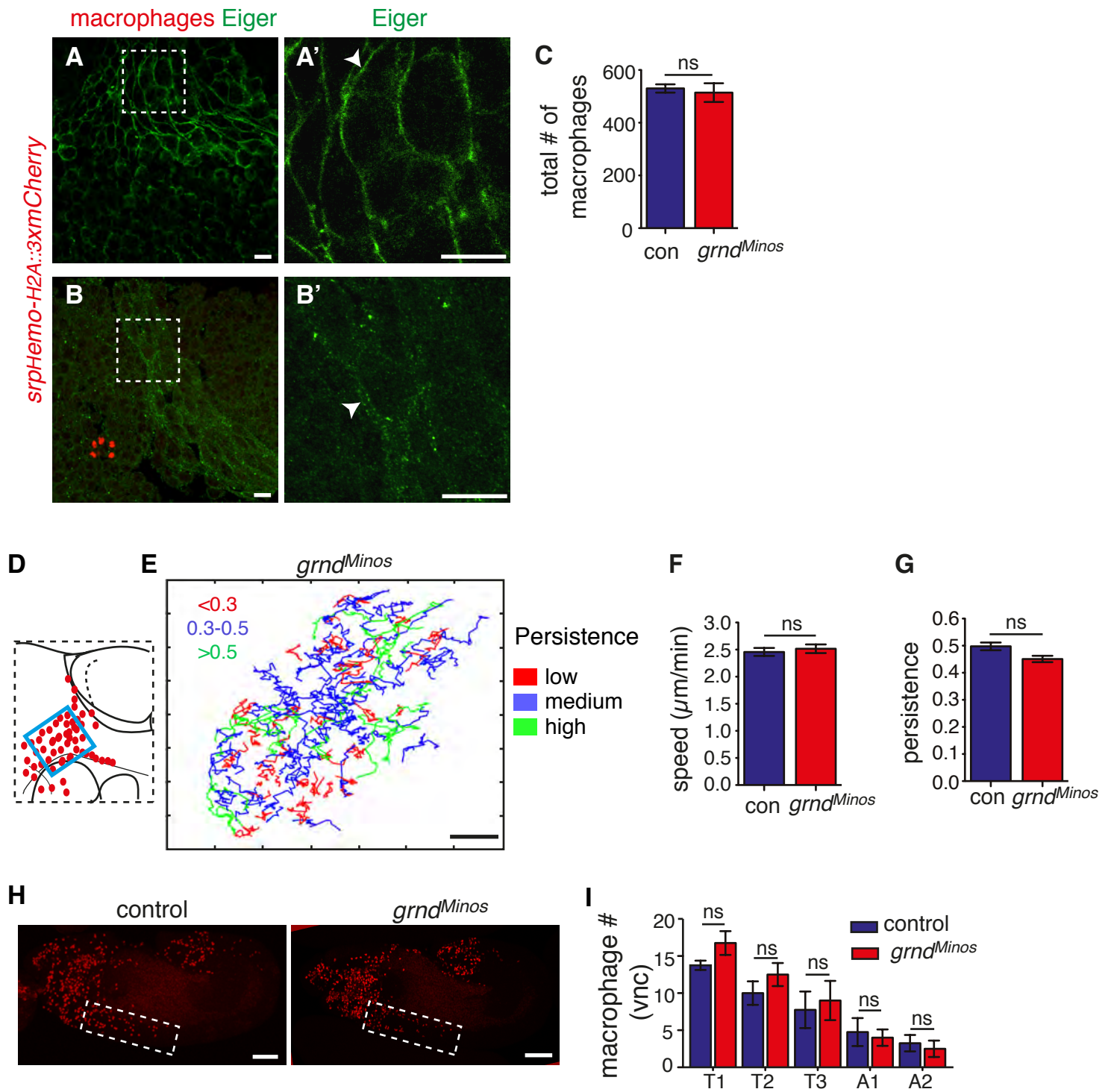


**Figure S3: Grindelwald does not affect general macrophage migration. Related to Figure 3.**

(A,B) Confocal images of a single sagittal section, from the same location as Figure 3A,B but at a position along the Z-axis that is closer to the viewer, in which the amnioserosa extends more broadly across the embryo in the anterior posterior direction, thus more extensively covering the germband ectoderm. Images are of (A,A') a lateral control Stage 10 and (B,B') a Stage 11 embryo with macrophage nuclei labeled by the expression of *srpHemo-H2A::3XmCherry* (red) and Eiger recognized with an antibody (green). Right panels show a magnification of the area indicated by the white dotted box in the adjoining panels on the left. (A') We observe punctate membrane expression of Eiger in AS cells in Stage 10 (arrowhead) and (B) much less in Stage 11.

(C) The total number of macrophages in the embryo in late Stage 12 is not significantly (ns) affected by the *grnd*<sup>Minos</sup> mutation. n=15 embryos for both genotypes.

(D) Schematic drawing of the anterior half of a lateral Stage 11 embryo indicating the region analyzed (area within blue box) to assess the persistence of macrophage migration up to the germband to produce the two-photon movie tracks shown on the right. The black dotted line within the germband in the schematic indicates the ectoderm-mesoderm interface. (E) Representative tracks of macrophages in *grnd*<sup>Minos</sup> embryos from cell tracking in the region shown in the blue box in D, color-coded according to low (<0.3; red), medium (0.3-0.5; blue) and high (>0.5; green) persistence of movement. (F,G) No significant change was observed in the *grnd*<sup>Minos</sup> mutant in speed or persistence. n=3 embryos for each genotype.

**(H)** Confocal microscopy images of Z-projections of fixed lateral late Stage 12 (greater than 45% retraction of the germband away from the anterior) control and *grnd*<sup>Minos</sup> mutant embryos are shown with macrophages labeled in red by the expression of *srpHemo-H2A::3xmCherry*. The dotted area indicates the region quantitated to determine macrophage migration along the ventral nerve cord (vnc).

**(I)** Quantification of the number of macrophages in each indicated thoracic (T1-3) or abdominal (A1-2) segment along the vnc. No significant difference was seen when comparing control and *grnd*<sup>Minos</sup> embryos. n=15 embryos for both genotypes.

Anterior to left and dorsal up in all panels. Embryos were selected for Stage 10 if they displayed germband retraction away from the anterior of less than 29%, Stage 11 if they displayed germband retraction away from the anterior of 29-31% and for Stage 12 retraction of 35-40%. Scale bar represents 10 $\mu$ m in **A-B',E** and 50 $\mu$ m in **H**. Histograms show mean  $\pm$  s.e.m. ns=not significant. Unpaired t-test for **C** and **I** and One-Way ANOVA with Dunnett post test for **F** and **G**.

Figure S4

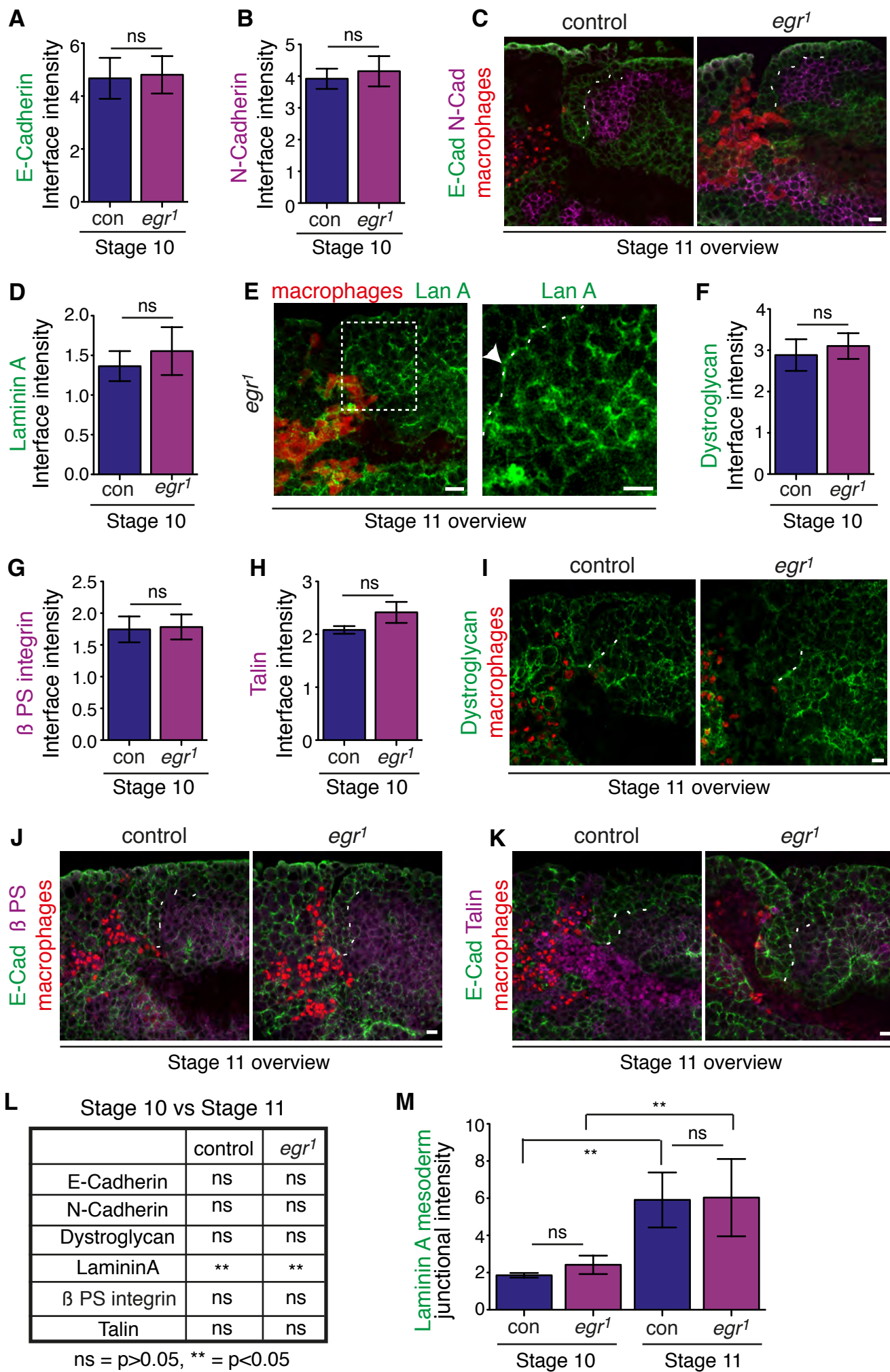


**Figure S4: Eiger (Dm-TNF) does not regulate adhesion at the ectoderm-mesoderm interface. Related to Figure 4.**

(A,B,D,F-H) Quantitation of the (A) E-Cadherin, (B) N-Cadherin, (D) Laminin A (LanA), (F) Dystroglycan, (G)  $\beta$ -PS integrin, and (H) Talin levels at the ectoderm-mesoderm interface in Stage 10 control (con) and *egr<sup>1</sup>* mutant embryos.

(C,E,I-K) Confocal images of the germband ectoderm [area in schematic in (Figure 4A)] from a single sagittal plane of fixed lateral Stage 11 control and *egr<sup>1</sup>* mutant embryos showing staining with an antibody against (C) E-Cadherin (green) and N-Cadherin (magenta), (E) LanA (green), (I) Dystroglycan (green) or (J,K) DE-Cadherin in green and (J)  $\beta$ -PS integrin or (K) Talin in magenta. Macrophages labeled in red by the expression of *srpHemo-3xmCherry* (*egr<sup>1</sup>* mutant in C,E) or *srpHemo-H2A::3xmCherry*. Dotted lines indicate the ectoderm-mesoderm interface.

(L) A table showing a comparison of the levels of adhesive proteins at the ectoderm-mesoderm interface between Stage 10 and Stage 11 for both control and *egr<sup>1</sup>* mutant embryos.

(M) Quantitation of the junctional LanA levels in the mesodermal junctions in Stage 10 and Stage 11 control (con) and *egr<sup>1</sup>* mutant embryos.

Anterior to left and dorsal up in all panels..Embryos were selected for Stage 10 if they displayed germband retraction away from the anterior of less than 29% and Stage 11 if they displayed 29-31% retraction with macrophages at and near the edge of the germband. Scale bar represents 20 $\mu$ m in left panel in E and 10 $\mu$ m in all the other images.

Histograms show mean $\pm$ s.e.m. \*\*P<0.01, ns=not significant, Unpaired t-test for A,B,D,F-H,L and One-Way Anova with Tukey post test in M.

Figure S5

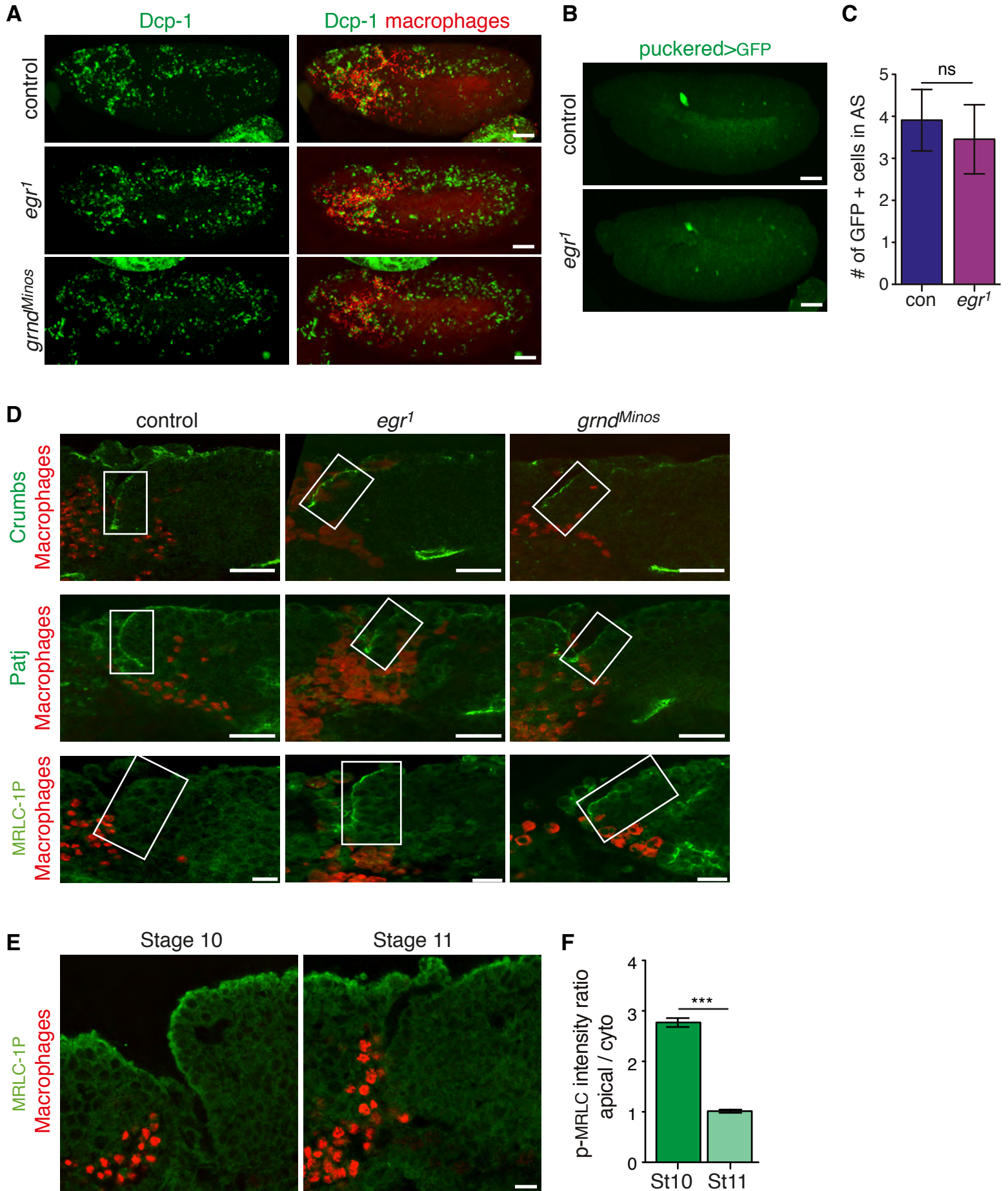




**Figure S5: Eiger and Grindelwald do not regulate cell death and JNK activity to support macrophage germband invasion. Related to Figure 5.**

(A) Confocal microscopy images of Z-projections of fixed lateral Stage 12 control, *egr<sup>1</sup>* mutant and *grnd<sup>Minos</sup>* mutant embryos with apoptotic nuclei visualized by antibody staining against Dcp-1 (green) and a merge showing macrophages visualized by *srpHemo-3XmCherry* expression (red) along with the apoptotic nuclei (green).

(B) Confocal microscopy images of Z-projections of fixed lateral Stage 11 control, (*UAS-GFP; srpHemo-3XmCherry pucE69-GAL4*) and *egr<sup>1</sup>* mutant embryos (*UAS-GFP egr<sup>1</sup>; srpHemo-H2A::3XmCherry pucE69-GAL4*) with JNK activity visualized by the *pucE69-GAL4 UAS-GFP* reporter.

(C) Quantification of the number of GFP positive cells in the amnioserosa in the control (con) and *egr<sup>1</sup>* mutant embryos. n=15 embryos for both genotypes.

(D) Confocal images of the germband ectoderm [area in schematic in (Figure 5D)] from a single sagittal plane of lateral Stage 12 fixed embryos from control, *egr<sup>1</sup>* and *grnd<sup>Minos</sup>* embryos immunolabeled for Crumbs, Patj or a phosphorylated form of Myosin Regulatory Light Chain (p-MRLC, also called Sqh-1P) and macrophages labeled by the expression of *srpHemo-H2A::3xmCherry* or *srpHemo-3XmCherry*. Magnifications of the boxed areas from the images are shown in Figure 5 D,F,H.

(E) Confocal images of the germband ectoderm [area in schematic in Figure 5C] from a single sagittal plane of fixed lateral Stage 10 or Stage 11 embryos, showing staining with an antibody against Sqh-1P in green and macrophages labeled in red by the expression of *srpHemo-H2A::3xmCherry*. (F) Quantification of apical Sqh-1P levels in the germband ectoderm normalized to the cytoplasmic levels in Stage 10 and Stage 11 embryos. n=5 embryos, 42 contacts for both genotypes.

Anterior to left and dorsal up in all panels. Embryos were selected for Stage 10 if they displayed germband retraction away from the anterior of less than 29%, Stage 11 for displaying germband retraction away from the anterior of between 29-31%, with macrophages at and near the edge of the germband, and Stage 12 with 35-40% retraction. Scale bar 50 $\mu$ m in **A,B**, 20 $\mu$ m in **D**, and 10  $\mu$ m in **E**. Histograms show mean  $\pm$  s.e.m. ns=not significant, \*\*\*P<0.001. Unpaired t-test for **C,F**.

Figure S6

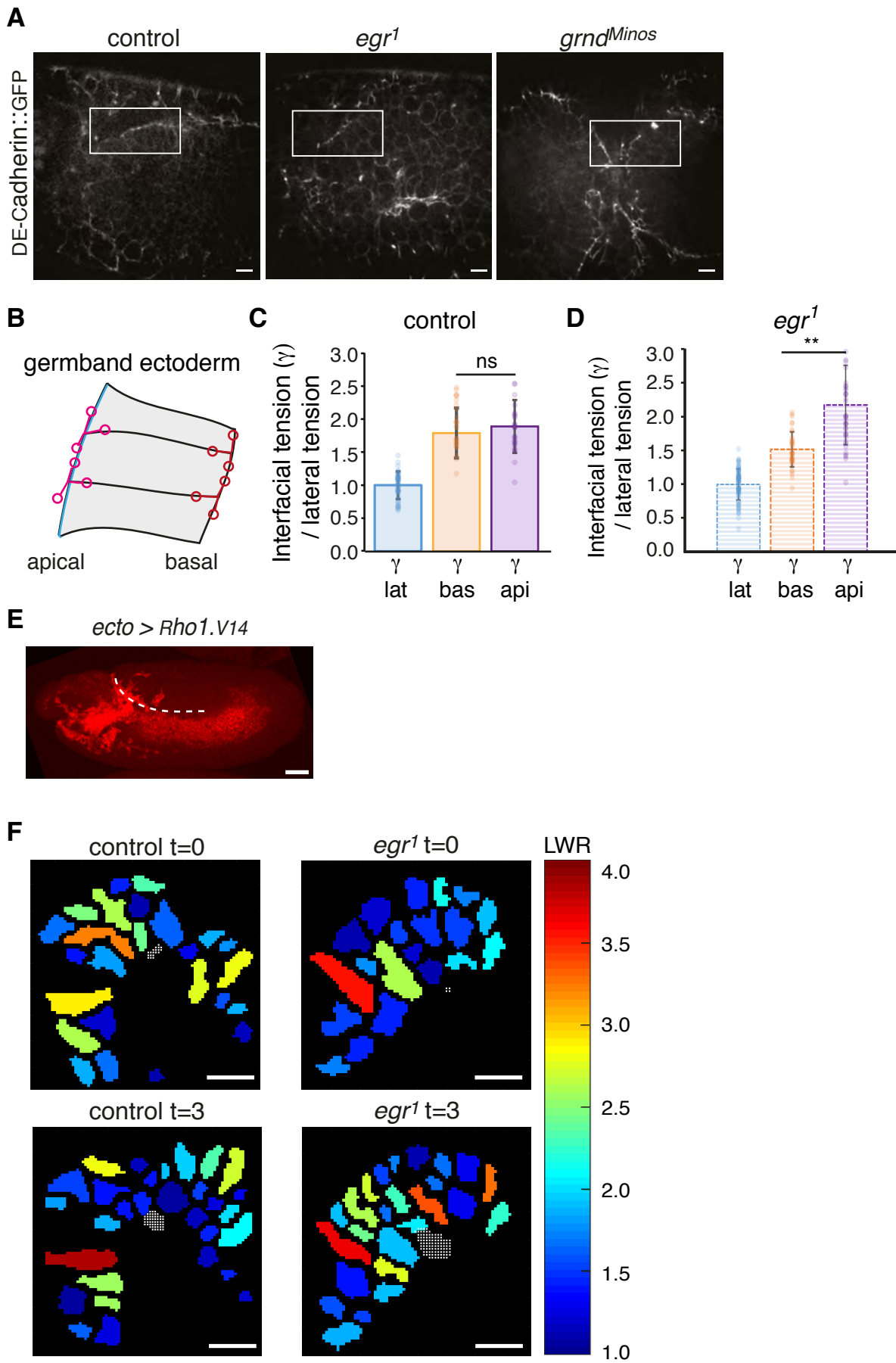


**Figure S6: Eiger regulates ectodermal cortical tension and facilitates ectoderm cell deformations. Related to Figure 6.**

(A) Spinning disc images of control, *egr<sup>1</sup>* and *grnd<sup>Minos</sup>* embryos labeled with *knock in DE-Cad::GFP*. Boxes indicate the region where the laser cuts were conducted.

(B) Schematic of a few cells from the germband ectoderm showing representative cell triple interfacial junctions at apical (magenta) and basal (brown) interfaces, as part of the CellFIT-3D based tension analysis.

(C,D) Interfacial tensions of the germband ectoderm determined by CellFIT-3D analysis. Interfacial tensions in Stage 11 (C) control and (D) *egr<sup>1</sup>* mutant embryos of the lateral, basal and apical regions are shown normalized to the tension of the lateral side.

(E) Confocal microscopy image of a fixed lateral Stage 12 embryo carrying *e22c-GAL4* to drive ectodermal expression of a dominant active form of Rho1 (*UAS-Rho1.V14*) in an embryo with *srpHemo-3XmCherry* labeling macrophages. n=20 embryos for both genotypes.

(F) Representative time points (t=0 and t=3, see **Figure 6H**) from time-lapse analysis of ectodermal cell deformation during macrophage entry in control and *egr<sup>1</sup>* embryos. The length/ width ratio (LWR) of the ectodermal cells is shown color-coded according to the scale on the right; the white dotted region is the macrophage.

Embryos shown with anterior to the left and dorsal up. Embryos were selected as Stage 11 for displaying germband retraction away from the anterior of between 29-31%, with macrophages at and near the edge of the germband, and Stage 12 with 35-40% retraction. Histograms show mean  $\pm$  s.e.m. \*\*P<0.01, Unpaired t-test for C,D. Scale bar represents 50 $\mu$ m in E and 10 $\mu$ m in A,F.